660 *Chem. Mater.* **2010,** *22,* 660–674
DOI:10.1021/cm902640j

CHEMISTRY OF MATERIALS
Review

Materials for Solid Oxide Fuel Cells[†]

Allan J. Jacobson*

Department of Chemistry, University of Houston, Houston, Texas, 77204-5003

Received August 26, 2009. Revised Manuscript Received October 9, 2009

Solid oxide fuel cells (SOFCs) have the promise to improve energy efficiency and to provide society with a clean energy producing technology. The high temperature of operation (500−1000 °C) enables the solid oxide fuel cell to operate with existing fossil fuels and to be efficiently coupled with turbines to give very high efficiency conversion of fuels to electricity. Solid oxide fuel cells are complex electrochemical devices that contain three basic components, a porous anode, an electrolyte membrane, and a porous cathode. In this short review, a survey of the types and properties of materials that have been considered for each of these components is presented with an emphasis on the requirements for operation at intermediate temperature (500−800 °C). Some directions for future research are discussed.

1. Introduction

Solid oxide fuel cells (SOFCs) have the promise to improve energy efficiency and to provide society with a clean energy producing technology. The high temperature of operation (500−1000 °C) enables the solid oxide fuel cell to operate with existing fossil fuels to give very high efficiency conversion of fuels to electricity and to be used in combined heat and power applications or efficiently coupled with gas turbines. SOFCs are quiet and nonpolluting and their inherent high efficiency leads to lower greenhouse gas emissions.[1−4]

Solid oxide fuel cells are complex electrochemical devices that contain three basic components, a porous anode, an electrolyte membrane, and a porous cathode. A schematic representation of an electrolyte supported solid oxide fuel cell is shown in Figure 1a. In this particular design, the dense electrolyte membrane supports the porous electrodes. The cathode is typically an oxide that catalyzes the oxygen reduction reaction:

$$1/2O_2(g) + 2e^- \rightarrow O^=(s)$$

The anode catalyzes the oxidation of fuel, either hydrogen or reformed hydrocarbons:

$$H_2(g) + O^= \rightarrow H_2O + 2e^- \text{ and } CO(g) + O^= \rightarrow CO_2 + 2e^-$$

The dense electrolyte membrane separates the air and fuel compartments and is a pure oxygen ion conductor. Oxygen from air is supplied on one side of the cell and hydrogen and carbon monoxide from reformed hydrocarbon fuel on the other side. The electrodes provide the interface between chemical and electric energy and catalyze the chemical reactions. Ideally, these reactions should be very fast (at equilibrium) to minimize voltage losses; high current requires fast reaction rates and high fluxes of molecules, ions, and electrons. As shown schematically in Figure 1b, the oxygen chemical potential difference between air and fuel is distributed across the cell and the output voltage depends on the magnitude of the overpotentials at the electrodes. For compound electrodes, their properties (for example, electronic conductivity and oxygen vacancy concentration) depend on the effective chemical potential they "see" and the chemical potential of the cathode is coupled to that of the anode. An individual cell produces ~1.0 V on open circuit and ~0.6−0.7 V under load. Multiple cells are connected together with bipolar plates to form a fuel cell stack that provides the output voltage appropriate for a particular application. The large gradient in the oxygen partial pressure across the cell from 0.2 atm on the air side to 1×10^{-15} to 1×10^{-20} atm on the fuel side places severe constraints on the choice of materials in terms of stability, chemical reactions at the interfaces, and compatible thermal expansion coefficients.

In the 1990s, solid oxide fuel cells operating at 1000 °C using an yttria stabilized zirconia electrolyte (YSZ), a lanthanum strontium manganite cathode, and a nickel−YSZ cermet anode were developed. Cells were connected by a lanthanum strontium chromite bipolar plate. Various geometries for the cell design were investigated but the most developed is the Siemens−Westinghouse tubular configuration in which the YSZ electrolyte film (30−40 μm) is supported on a 1.5 m long tube of porous lanthanum strontium manganite. The Siemens−Westinghouse design has been demonstrated successfully at the 100 kW scale.[5]

In recent years, the focus of SOFC development has been on lowering the operating temperatures of SOFCs to

[†] Accepted as part of the 2010 "Materials Chemistry of Energy Conversion Special Issue".

*Corresponding author. E-mail ajjacob@uh.edu. Tel: (713) 743-2785. Fax: (713) 743-2787.

 Published on Web 11/20/2009

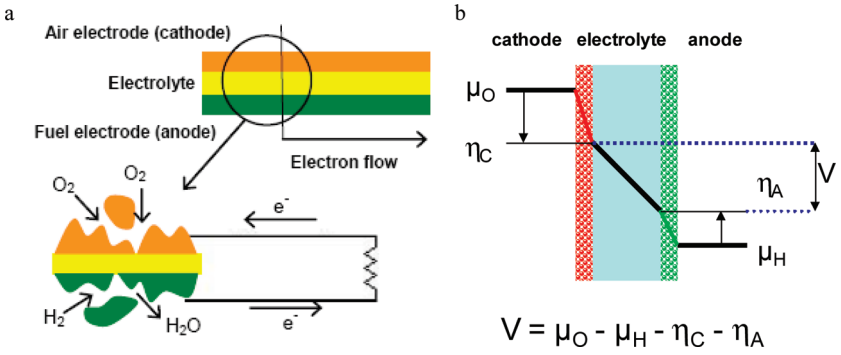

Figure 1. (a) Schematic of a single solid oxide fuel cell; (b) schematic diagram illustrating the drop in oxygen chemical potential across a single cell.

500 − 800 °C in order to reduce costs. Lowering the operating temperature has a significant impact on cost by allowing the use of less expensive materials in interconnects and heat exchangers. Lower temperatures also lead to an increase in the durability of SOFC systems by reducing problems associated with thermal cycling and performance degradation because of interdiffusion or reaction of the individual components. Operation at lower temperature, however, creates a number of materials problems that are associated with the increase in the electrolyte resistance and decrease in the rates of the electrocatalytic reactions (electrode polarization). Both factors result in a reduction of the cell voltage and output power. Finding new combinations of electrolyte and electrode materials that reduce these losses and provide both rapid ion transport across the electrolyte and electrode−electrolyte interfaces and efficient electrocatalysis of the oxygen reduction and fuel oxidation reactions remains a significant materials challenge. A fundamental atomistic level understanding of the factors that control bulk ionic mobility and trapping of defects, for example, in perovskites with high ionic conductivity such as the ordered double perovskite $PrBaCo_2O_{5+x}$[6] and doped lanthanum gallates[7] is needed to increase the likelihood of finding new materials combinations. The transport reaction network in the porous three-phase electrode structure is very complex and consequently how the properties of the electrode material determine the relative rates and contributions from the various processes and the overall electrode performance is not completely understood. Many different interfaces play a role in materials used in high-temperature electrochemical devices. There are homogeneous interfaces such as grain boundaries, which can have a deleterious effect upon the transport of ions in polycrystalline materials, and heterogeneous interfaces in materials such as polycrystalline composites. The study of stability (structure) of electrodes and interfaces under real operating conditions and the role that defects play in controlling mobility remain important areas for research.

2. Materials Properties

One way to think about the materials properties for the individual cell components is to put some approximate numbers on the desired performance.[8,9] If we assume that a single cell is required to deliver 0.7 A at 0.68 V, that is a power density of 490 mW/cm^2, then the total voltage polarization from the open circuit value is ~0.32 V made up of $iR+\eta_a+\eta_c$, where i is the current through the cell, R is the ohmic resistance, and η_a, η_c are the anodic and cathodic overpotentials, respectively. This constraint gives a single cell resistance of ~0.45 ohms cm^2 neglecting concentration polarization effects. In a fuel cell stack, the resistance will be higher because of additional losses from interconnects and the interfaces between them and the cell. The consequence of this power density requirement is to place a resistance limitation of ~0.15 ohms cm^2 on each individual cell component though the distribution in practice depends on the cell geometry (anode, cathode, or electrolyte supported).

2.1. Electrolytes. The general requirements for an electrolyte are high ionic conductivity, low electronic conductivity, stability in both oxidizing and reducing environments, good mechanical properties and long-term stability with respect to dopant segregation. Three electrolyte systems namely yttria stabilized zirconia (YSZ), strontium, magnesium-doped lanthanum gallate (LSGM), and gadolinium- or samarium-doped ceria (CGO or CSO) have been widely investigated for SOFCs. The minimum temperature at which each of these systems can be operated depends on a combination of the ionic conductivity and a realistic assessment of a minimum film thickness that can be reliably manufactured. Thus, if we assume a film thickness of 10 μm and a conductivity of 1×10^{-2} S cm^{-1} (corresponding to an area specific resistance of 0.1 ohms cm^2), then the minimum operating temperatures are ~700 °C (YSZ), ~550 °C (LSGM), and ~550 °C (CGO) based on the data in Figure 2.

Each electrolyte system offers advantages and disadvantages. Thus, YSZ fulfills the electrical requirements at high temperatures and has good high temperature mechanical properties. Problems occur because of its reactivity with perovskite oxide electrodes containing lanthanum at high temperature forming $La_2Zr_2O_7$ resistive layers. LSGM has higher ionic conductivity than YSZ and is more compatible with lanthanum transition-metal oxide perovskite cathodes. On the anode−electrolyte side, composite LSGM−NiO anodes are less compatible with LSGM because of the reactivity of NiO, than the corresponding composite Ni-YSZ anodes are with YSZ. Ceria

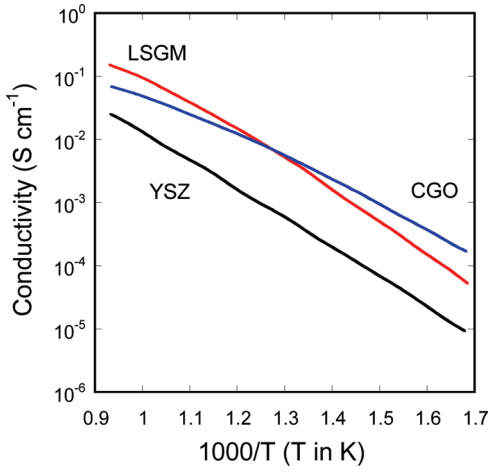

Figure 2. Conductivity data for YSZ,[2] CGO,[8] and LSGM.[10]

doped with rare earth metals has received considerable attention as an alternative electrolyte and it has the highest conductivity at lower temperature of other than doped bismuth oxides when substituted with 0.1−0.2 Gd_2O_3 or Sm_2O_3. Doped ceria is more stable than bismuth oxides but, in reducing conditions ($pO_2 \approx 1 \times 10^{-19}$ atm), Ce^{4+} is reduced to Ce^{3+}. The reduction reaction results in the introduction of electronic conductivity thereby reducing the fuel cell efficiency. The width of the electrolytic domain increases as the temperature is lowered and the electronic conductivity is no longer a problem at 500 °C.

2.2. Electrodes. Electrodes are critical components in SOFCs in that they provide the interface between the chemical energy associated with fuel oxidation and electrical power. Typically, they are complex structures that consist of a three-phase percolating composite of a metal or mixed conducting oxide, an oxide electrolyte and the pore space. The transport reaction network in such porous structures is very complex and consequently understanding of how the properties of the individual components determine the relative rates and contributions from the various processes and thereby the overall electrode performance have been studied by many groups. Several materials requirements are general to both anodes and cathodes. Both electrodes must have high (electro)catalytic activity and electronic conductivity to minimize the effective resistance. The anode acts as an electrocatalyst for the oxidation of fuel components by oxide ions transported through the electrolyte and the cathode catalyzes the oxygen reduction reaction. Electrons produced or consumed by the chemical reactions at the electrode surfaces must be transported to or from the external circuit. The electrodes must also be stable. Because a SOFC is cycled between room temperature and the operating temperature, the thermal expansion of the electrode must be matched to that of the electrolyte and the current collector to give stable interfaces. The electrodes must be chemically stable at the operating temperature with respect to the electrolyte and the current collector and must have stable microstructures under operating conditions with respect to both porosity and surface area.

Operation of SOFCs at intermediate temperatures requires improvement in electrodes that are compatible with a specific electrolyte. The manganese oxide cathode material $La_{0.9}Sr_{0.1}MnO_3$ (LSM) developed for operation with YSZ at high temperatures has adequate electronic conductivity at 1000 °C, is stable under oxidizing conditions, and has a good thermal expansion match with YSZ. At lower operating temperatures, however, the cathodic polarization with LSM electrodes is substantial in part because of the poor ionic conductivity. Reducing the temperature from 1000 to 500 °C gives an increase in the polarization resistance of LSM from < 1 to 2000 ohm cm^2, way outside of the practical range. New compositions and structures with much lower polarization resistances are required for SOFCs operating at 500−700 °C. The anode situation is similar. The state-of-the art anodes used with YSZ electrolytes are composites of nickel metal with YSZ as the ionically conducting component. These are widely used and the best available but have problems with stability on cycling, and when used with reformed hydrocarbon fuels, sulfur tolerance and carbon formation are issues. In addition to the electrochemical characteristics, other issues such as thermal expansion coefficients limit the choice of materials. For example, the usefulness of some of the best cathode materials containing cobalt is restricted because of their large thermal expansion coefficients ($> 20 \times 10^{-6}$ K^{-1}) relative to the common electrolytes.

Table

electrolyte	thermal expansion coefficient (K)
YSZ	10.8×10^{-6}
CGO	13.5×10^{-6}
LSGM (2020)	11.1×10^{-6}

In the remainder of this review, the status and some recent advances in electrode and electrolyte materials will be described. The discussion is not intended to provide a comprehensive review but to highlight particular materials of interest and to indicate areas of opportunity for new materials chemistry. References are provided to more comprehensive reviews, for example, cathodes,[11,12] anodes,[13] electrolytes,[14] and others are detailed in specific sections.

3. Components of Solid Oxide Fuel Cells

3.1. Electrolytes. The large number of oxygen ion electrolytes that have been investigated can be grouped into a small number of structure types: fluorite-based systems (doped bismuth oxide, zirconia, ceria, pyrochlore);[15] perovskite and related intergrowth structures (lanthanum gallate, brownmillerites, BiMeVOX);[16] LaMOX and apatites. All have some limitations and so the search for better systems continues. Many oxide conductors show order−disorder phase transitions and only show high conductivity above the transition where the oxygen ion sublattice "melts", at least to some degree. In these cases, suitable doping can suppress the phase transition and lead to higher conductivities at lower temperature.

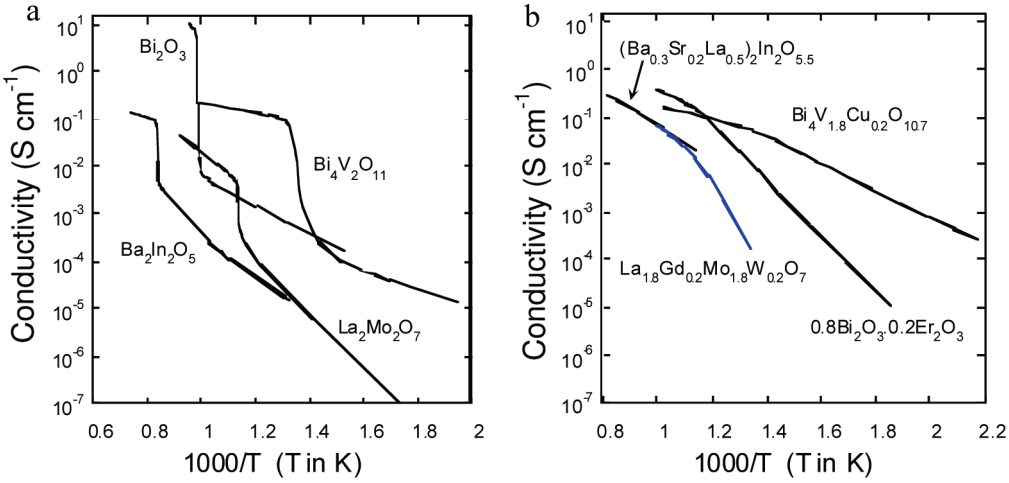

Figure 3. Examples of compounds showing (a) order−disorder transitions and (b) their doped counterparts. Data are taken from: Bi_2O_3,[17] $Bi_4V_2O_{11}$,[16] $Ba_2In_2O_5$,[48] $La_2Mo_2O_7$,[64] 0.8 $Bi_2O_3 \cdot 0.2Er_2O_3$,[20] $Bi_4V_{1.8}Cu_{0.2}O_{10.7}$,[16] $(Ba_{0.3}Sr_{0.2}La_{0.5})_2In_2O_5$, and [53] $La_{1.8}Gd_{0.2}Mo_{1.8}W_{0.2}O_7$.[68]

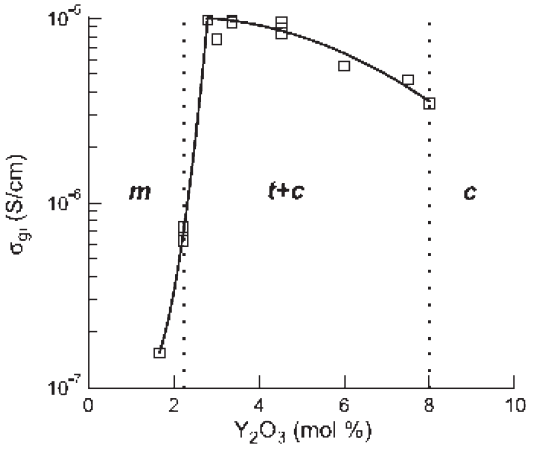

Figure 4. Ionic conductivity of $ZrO_2-Y_2O_3$ solid solutions at 300 °C. Reproduced with permission from ref 44. Copyright 2004 Elsevier.

All such compounds and others such as doped ceria and zirconia, which although they do not show macroscopic phase transitions, show evidence for vacancy-dopant short-range order apparent in non-Arrhenius behavior of the conductivity with temperature. Defect cluster growth and ultimately phase segregation are also observed on long-term annealing. Representative examples of conductivity behavior are shown in Figure 3 both for the parent phases that show order−disorder transitions and their doped counterparts.

3.1.1. Bismuth Oxide. Of the known oxide-ion conductors, high-temperature δ-Bi_2O_3 has the highest conductivity, >1 S/cm at 800 °C, but is stable only between 730 °C and its melting point at 804 °C. The δ-Bi_2O_3 phase has a fluorite-related structure with a random distribution of oxygen ions. At room temperature, the oxygen vacancies are ordered but on heating above 730 °C, a first-order vacancy order−disorder transition occurs and the conductivity increases by nearly 3 orders of magnitude. Takahashi et al.[17,18] demonstrated that the δ-phase can be stabilized to lower temperatures by partial substitution for Bi though dopants lower the conductivity. For example, with Y_2O_3, the δ phase is stable in the composition range 25−43 mol % Y_2O_3 over a wide range of temperatures. The highest conductivities of $(Bi_2O_3)_{0.75}$-$(Y_2O_3)_{0.25}$ are 1.6×10^{-1} ohm cm^{-1} at 700 °C and 1.2×10^{-2} ohm cm^{-1} at 500 °C. Erbium oxide doping gives even higher conductivities the best being found for $(Bi_2O_3)_{0.8}(Er_2O_3)_{0.2}$ (see Figure 3b). The conductivities at 700 and 500 °C are 3.7×10^{-1} ohm cm^{-1} and 2.3×10^{-2} ohm cm^{-1}, respectively.[19,20] Unfortunately, the rare earth oxide stabilized phases transform at 600 °C to the vacancy-ordered rhombohedral phase which has a significantly lower conductivity.[21] Small additions of other oxides such as ZrO_2 have been reported to suppress this aging effect. The biggest problem with stabilized bismuth oxides for practical application is their instability with respect to reduction to bismuth metal under anode conditions. The use of bilayer structures with a more stable electrolyte layer (for example CGO or CSO) on the anode side has been suggested as an approach to solve this problem.[22]

3.1.2. Zirconia-Based Electrolytes. The properties of zirconia-based electrolytes with a variety of divalent and trivalent cation dopants have been studied for many years and their properties are well-described in a number of review articles.[23,24] From this work, yttria stabilized zirconia has become established as the preferred electrolyte. The bulk ionic conductivity measured at 300 °C of $ZrO_2-Y_2O_3$ solid-solution samples at low doping is shown in Figure 4. The phase boundary between the monoclinic solid-solution phase field and the tetragonal + cubic phase field occurs at 3 mol % Y_2O_3, where the conductivity increases dramatically. At 8 mol % Y_2O_3, the phase is cubic and this composition is the one that is usually used. The conductivity is ~0.1 S cm^{-1} at 1000 °C but operating at this high temperature gives rise to significant problems with other components. Yttria-stabilized zirconia does have good chemical and mechanical stability over a wide range of oxygen partial pressures and temperatures and consequently efforts to maintain the conductivity at temperatures in the 700−800 °C range by improvements in processing to control the microstructure are continuing. A discussion of recent results in this area can be found in progress reports available at the

Department of Energy Solid State Energy Conversion Alliance Web site.[25]

Scandia-stabilized zirconia (ScSZ) is an alternative to YSZ for use at intermediate temperature because of its higher conductivity.[26,27] ScSZ compositions with 8−12 mol % scandia have the highest oxide ion conductivities among all the zirconium oxides.[28] The ionic conductivity of the $ZrO_2-Ln_2O_3$ systems decreases with increasing Ln^{3+} radius and Arrhenius plots show curvatures characteristic of defect-dopant association. The high conductivity of ScSZ is attributed to the low association enthalpy of defects due to the similar radii of Sc^{3+} and Zr^{4+}. ScSZ (10−15 mol %) has a rhombohedral structure, which transforms to a cubic structure above 600 °C with higher conductivity. The cubic structure can be stabilized at room temperature by adding small amounts of other dopants such as Y_2O_3.[29]

3.1.3. Ceria-Based Electrolytes. In several ways, Gd- or Sm-stabilized ceria electrolytes are the most interesting candidates for intermediate temperature SOFCs (550−650 °C) both because of the high ionic conductivity and compatibility with high-performance electrode materials such as cobalt containing perovskite oxide cathodes.

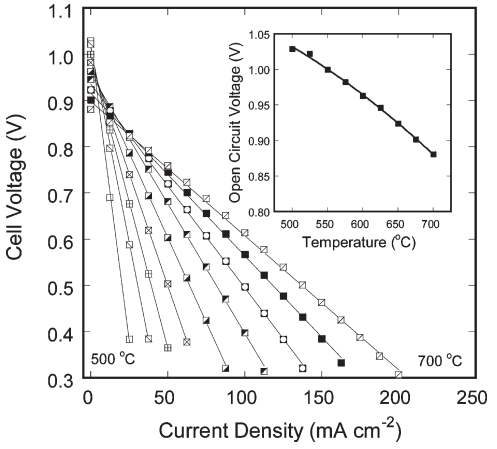

Figure 5. Results for a CGO electrolyte supported (0.8 mm thick) solid oxide fuel cell with 97 vol % H_2 + 3 vol % H_2O, Ni-CGO anode/CGO electrolyte/PBCO-CGO cathode, air from 500 to 700 °C at 25 °C intervals. The inset is the temperature dependence of the open circuit voltage.

The conductivity in air of rare-earth-doped ceria has been reviewed in detail.[8,30,31] An important disadvantage of doped ceria electrolytes is they become n-type electronic conductors under reducing conditions and the cell output voltage is reduced (see Figure 5).[32−35] Although Gd- and Sm-doped cerias are generally recognized as the better conductors and hence typically used, excellent conductivity has been observed in yttria-doped ceria.[36] At 750 °C, the conductivities are comparable with values of $\sigma = 6.5 \times 10^{-2}$ S cm^{-1} for CYO,[36] 6.7×10^{-2} S cm^{-1} for CGO,[37] and 6.1×10^{-2} S cm^{-1} for CSO.[38] At this level of comparison, differences are most likely due to the presence of impurities at grain boundaries and differences in microstructure. Thus CYO may compare favorably with CGO and CSO especially because in combination with a thin YSZ electrolyte layer, CYO should not have interdiffusion problems at high temperature.

To improve the properties of ceria-based materials, particularly the stability at low pO_2, and sinterability, a number of approaches have been taken to find the ideal dopant and dopant concentration and to improve materials processing by the introduction of specific sintering aids. Several codoped ceria electrolytes have been investigated, for example, $Ce_{0.85}Gd_{0.1}Mg_{0.05}O_{1.9}$,[39] $Ce_{1-a}Gd_{a-y}Sm_yO_{2-0.5a}$,[40] $Ce_{1-x-y}Gd_xPrO_{2-z}$,[41] $Ce_{0.8}Sm_{0.2-x}Y_xO_{1.9}$,[42] and $Ce_{0.8}Gd_{0.2-x}Y_x$[43] with some positive results. Results for the $Ce_{0.8}Gd_{0.2-x}Y_x$ system are shown in Figure 6. At 600 °C the oxygen partial pressure when $\sigma_i = \sigma_e$ is 8.7×10^{-21} atm for pure CGO and decreases to 1.9×10^{-21} atm at $x = 0.15$. As can be seen from the figure the enhanced stability is obtained at the cost of a reduction in the ionic conductivity. Nevertheless, the results suggest that addition studies to optimize the dopants and to understand how they affect the properties are warranted.[44]

The influence of additives on the sintering of ceria at lower temperature and processing into thin layers are of current interest. Some transition metal oxides such as MnO_2, Fe_2O_3, and Co_3O_4, are known to be effective sintering aids. For example, densification of $Ce_{0.9}Gd_{0.1}O_{1.95}$, is strongly promoted by the addition of 1% of cobalt oxide, which lowers the maximum sintering temperature by 200 °C and increases the densification rate. This change in sintering behavior results from cobalt ion

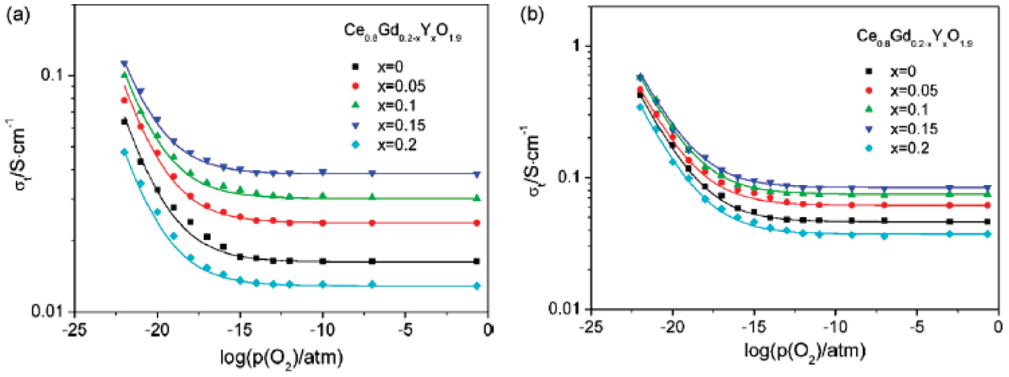

Figure 6. Total electrical conductivity of doped ceria as a function of oxygen partial pressure at (a) 873 and (b) 973 K. Solid lines show the dependence of $\sigma_t = \sigma_i + kpO_2^{-1/4}$. Reprinted with permission from ref 43. Copyright 2008 Elsevier.

segregated at the grain boundaries.[45] Silica is a common impurity in ceria electrolytes and is known to have a detrimental effect on the ionic conductivity by blocking at grain boundaries. A small addition of Fe_2O_3 has a scavenging effect on SiO_2 impurities, and it improves the grain boundary conduction of impure CGO20.[46]

In conclusion, doped ceria is a promising electrolyte material for fuel cells operating between 500−650 °C. High-performance cathode materials for CGO have been demonstrated, but more work is needed on densification and on high performance anodes.

3.1.4. Perovskite Related Systems. Oxygen deficient perovskite oxides are the fourth major category of electrolyte materials. The ionic conductivities of a large number of compounds have been reviewed and the conductivity data analyzed in terms of the perovskite tolerance factor, degree of oxygen nonstoichiometry, and the type of A and B site cation substitutions.[47] Systems based on the brownmillerite structure have been studied since the observation of the order−disorder transition in $Ba_2In_2O_5$ above 925 °C.[48] Above this temperature a disordered cubic structure is formed with pure oxygen ion conductivity.[49] Calorimetric measurements show that the entropy change at the transition is only 4% of that calculated for a complete order−disorder transition. This residual short-range order appears to be typical of brownmillerite to perovskite phase transitions and similar results are found for $Sr_2Fe_2O_5$.[50] In contrast, the entropy increase at the transition to δ-Bi_2O_3 is much larger and the oxygen sublattice becomes more "liquid"-like with a correspondingly larger increase in conductivity at the phase transition. Following the work on brownmillerite, other intergrowth phases with different numbers of octahedral and tetrahedral layers, for example, ($Ba_3In_2MO_8$) (M = Ce, Hf and Zr), were investigated.

In $Ba_2In_2O_5$, many other substitutions were made to suppress the phase transition.[51,52] The oxygen ion conductivity of the composition $(Ba_{0.3}Sr_{0.2}La_{0.5})InO_{2.75}$ is probably the best, reaching a value of 0.12 S cm^{-1} at 800 °C (see Figure 3) exceeding that of yttria-stabilized zirconia.[53,54] The performance of this electrolyte was evaluated in an SOFC with Pt and Ni electrodes and gave a respectable peak power density of ~0.5 W/cm^2 at 800 °C.

Following the work on the barium indium oxide phases, the groups of Ishihara[55,56] and Goodenough[57,58] made a significant advance in the perovskite class of electrolytes with the discovery of the double substituted (La,Sr)(Ga,Mg)O_{3-x} (LSGM) compositions. In early work, Ishihara showed that the oxygen ion conductivity of $La_{0.9}Sr_{0.1}Ga_{0.8}Mg_{0.2}O_{3-x}$ was greater than that of Sc-doped ZrO_2 and that electronic conductivity was negligibly small in the oxygen partial pressure region from 1 to 1×10^{-20} atm.

Independently, Goodenough reported an oxygen ion conductivity of $\sigma > 1 \times 10^{-2}$ S cm at 600 °C for $La_{0.9}Sr_{0.1}Ga_{0.8}Mg_{0.2}O_{2.85}$ with a transport number $t \approx 1$ over the same pO_2 range. The conductivity deviates from Arrhenius behavior above 600 °C; below 600 °C the apparent activation energy is 1.07 eV slightly larger than the 0.98 eV of YSZ. The thermal-expansion coefficient is similar to that of yttria-stabilized zirconia (YSZ). Subsequently, the solid solution range was investigated in more detail[59−62] and the conductivity determined as a function of composition. The highest values of $\sigma = 0.17$ and 0.08 S/cm were found for $La_{0.8}Sr_{0.2}Ga_{0.83}Mg_{0.17}O_{0.2815}$ at 800 and 700 °C, respectively. The data for this composition are shown in Figure 2. Although, the conductivity of LSGM has been reported to be stable over extended periods, the chemical stability under reducing conditions at high temperature remains a question. In one study in humidified hydrogen at 1000 °C,[63] significant changes were observed in the surface morphology of the electrolyte, and $La(OH)_3$, $LaSrGaO_4$, and some unknown phases were formed as a result of the vaporization of Ga_2O. Other issues concerning the reactivity of LSGM with electrode materials are discussed below.

3.1.5. $La_2Mo_2O_9$ (LAMOX). $La_2Mo_2O_9$ (LAMOX) is an oxygen ion conductor first reported by Lacorre et al. in 2000 that shows an oxygen ion conductivity greater than that of yttria-stabilized zirconia (YSZ).[64] LAMOX is subject to a structural phase transition from a nonconductive monoclinic α form to the highly conductive cubic β form at about 580 °C similar to that observed in Bi_2O_3. The conductivity increases by almost 2 orders of magnitude and is $\sim 6 \times 10^{-2}$ S cm^{-1} at 800 °C. Because of the phase transition and the possible reducibility of molybdenum, a number of substitutions for both lanthanum and molybdenum have been made in order to suppress the phase transition and improve the stability in reducing environments for practical applications.[65−68] A wide range of substitutions for La have been reported, most of which stabilize the high-temperature β structure. For Nd substitution, the monoclinic α form is stable at room temperature in the whole compositional range, whereas for Gd and Y substitutions, a small substitution level suppresses the phase transition and stabilizes at room temperature the cubic β form. The phase stability under low oxygen partial pressure is improved though with reduction in the ionic conductivity by substituting molybdenum by tungsten which forms solid solutions $La_2Mo_{2-x}W_xO_9$ with $x \leq 1.6$. Tungsten-substituted $La_2Mo_2O_9$ compositions have been reported to show sufficient ionic conductivity and stability at 600 °C to be used as electrolytes.[69] The main problem with LAMOX is its reactivity toward electrode materials. Chemical compatibility studies with $La_2Mo_{2-y}W_yO_9$ ($y = 0.5$ and 1.5) revealed that CuO is more compatible than NiO as an anode material.[70] Ferrites seem to be the most physical and chemical compatible cathodes studied to date, although their polarization resistance is too large to consider their use in SOFCs. The practical application of $La_2Mo_{2-y}W_yO_9$ materials is rather limited because of their high chemical reactivity and high thermal expansion coefficients. The development of alternative electrodes compatible with LAMOX electrolytes is required or alternatively a protective buffer to suppress molybdenum diffusion.

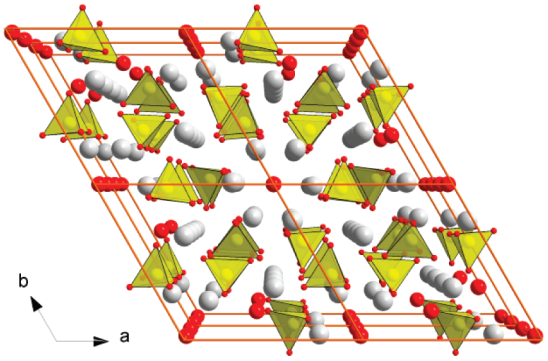

Figure 7. Representation of the structure of apatite viewed down the *c* axis; the XO_4 tetrahedra are yellow, the lanthanum and oxygen atoms are gray and red spheres.

Table 1. Conductivity of Some Lanthanum Silicate Apatites (data from ref 74)

compd	σ (S cm^{-1} at 500 °C)	E_a (eV)
$La_8Sr_2(SiO_4)_6O_2$	5.6×10^{-7} (800 °C)	1.14
$La_{9.33}(SiO_4)_6O_2$	1.1×10^{-4}	0.74
$La_{9.67}(SiO_4)_6O_{2.5}$	1.3×10^{-3}	0.62
$La_9Sr(SiO_4)_6O_{2.5}$	1.2×10^{-3}	0.56

3.1.6. Apatites. Rare-earth apatite materials have relatively high oxide ion conductivity at moderate temperatures as well as at low oxygen partial pressures[71−73] and have been proposed as alternative solid electrolyte materials following the initial work of Nakayama on the silicate-based systems.[74−76] The compounds have the general formula $M_{10}(XO_4)_6O_{2+y}$, where M is a rare-earth or alkaline earth metal and X is P, Si, or Ge. The hexagonal structure is illustrated in Figure 7 and comprises isolated XO_4 tetrahedra and columns of M cations and oxygen ions along the *c* axis forming two distinct channels.

The smaller of the channels contains lanthanum ions and vacancies, while the larger contain both lanthanum ions and the oxygen ions that are not part of the XO_4 tetrahedra. Lanthanum silicate apatites exhibit the highest conductivities and show pure oxygen ion conductivities over a wide range of oxygen partial pressures. The conductivity is anisotropic as expected from the structure with the largest value in the direction parallel to the *c* axis. A number of studies of chemical substitutions aimed at optimizing the ionic conductivity have shown that the apatites can tolerate a wide range of dopants and that the conductivity depends on the degree of anion and cation nonstoichiometry and the chemical nature of the dopant. Fully stoichiometric systems, such as $La_8Sr_2(SiO_4)_6O_2$, exhibit poor conductivity, whereas La vacancies in the small channels, for example, in $La_{9.33}(SiO_4)_6O_2$ (Figure 7) improves the conductivity. Samples containing oxygen excess and/or vacancies at the rare earth site, such as $La_{9.33+2x/3}(SiO_4)_6O_{2+x}$ ($x > 0$) and $La_9Sr(SiO_4)_6O_{2.5}$ show the highest conductivities. Representative data are given in Table 1

Perhaps the most interesting aspect of the apatite conductors is that, in contrast to the perovskite and fluorite-based compounds, in which conduction proceeds via oxygen vacancies, the conductivity in apatites involves interstitial oxide-ions. Atomistic simulations of the oxygen ion transport mechanism along the *c*-axis in $La_{9.33}(SiO_4)_6O_2$ and $La_{9.67}(SiO_4)_6O_{2.5}$ phases predict that oxygen ion conduction proceeds via an interstitial mechanism with a complex sinusoidal migration pathway at the periphery of the conduction channels and the presence of an energetically favorable oxygen interstitial site at the channel periphery.[77−80]

In the context of applications, it should be noted that high-quality apatite ceramics are not easy to make and very high temperatures are required to obtain dense samples (>1600 °C). Conventional synthesis methods also require high temperatures (>1300 °C) and development of better synthesis methods is needed.[81]

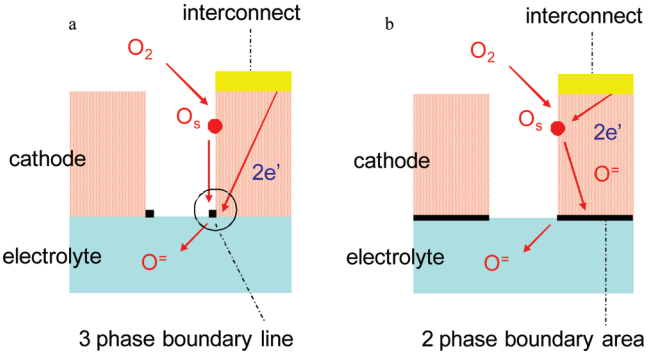

Figure 8. Schematic representations of cathode structures the cathode is a (a) poor or (b) good ionic conductor.

3.2. Cathodes. Two schematic models for the reactions that occur at cathodes are shown in Figure 8 for a single-phase cathode material to illustrate the various coupled reaction and transport processes that occur and the different types of interfaces that are present. The behavior of an electrode with low oxygen ion conductivity such as $La_{0.9}Sr_{0.1}MnO_3$ is qualitatively described in Figure 8a. The cathode reaction is represented by diffusion of oxygen gas into the pore space, dissociation, and diffusion to the triple phase boundary between gas phase, the electrode and the electrolyte and then ion transfer into the electrolyte.

A schematic of a mixed conducting cathode structure is shown in Figure 8b. Here, oxygen molecules diffusing into the porous structure are reduced to form ions at the surface of a mixed conducting cathode material and also at the triple phase boundaries between the current collector, cathode material and gas phase, and between the cathode material, electrolyte, and gas phase. The oxygen ions that are formed on reduction diffuse either through the cathode material or along the surface to the electrolyte, where they are transferred to the electrolyte either across the solid−solid interface between the cathode and the electrolyte or in the vicinity of the triple phase boundary. The mixed conductor would be expected to show lower resistance because of the larger area available for reaction and ion transfer across the interface. Gas-phase diffusion into the porous structure must also be considered and is known to become important at high

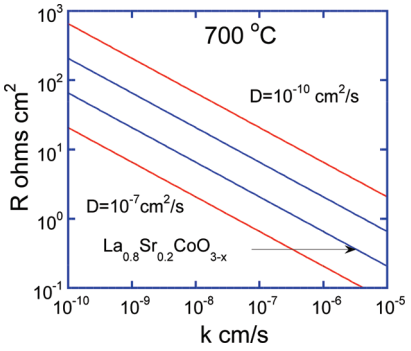

Figure 9. Variation of the area specific resistance with D and k calculated at 700 °C.

current densities. A more detailed discussion of modeling the performance of cathode materials can be found in recent reviews by Adler[11] and Liu.[12]

The models can be used to select new compounds based on intrinsic properties. For example, the ALS[82] model describes the electrode resistance in terms of the electrode microstructure (tortuosity, porosity, and surface area), the oxygen ion diffusion coefficient D, and the surface exchange velocity k at the appropriate oxygen pressure. By using this model, we can make a preliminary assessment of the likely effectiveness of a specific cathode material. Some estimates of the area specific resistance calculated assuming an electrode structure with a surface area of 10 000 cm^{-1}, a particle size of 3 μm, a porosity of 31%, and a tortuosity of 1.16 at 700 °C are shown in Figure 9.

The experimental (D, k) data for $La_{0.8}Sr_{0.2}CoO_{3-x}$ are indicated by the arrow and correspond to an area specific resistance of ~0.4 ohm cm^2. An increase by a factor of 10 in the surface area of the electrode would reduce the area specific resistance to 0.13 ohm cm^2 for $La_{0.8}Sr_{0.2}CoO_{3-x}$, a value that has been achieved for LSCO on CGO.[83]

What is not considered above is that the specific electrolyte plays an important role in determining the overall cathode performance. For example, Ralph et al.[84] examined a series of perovskite compositions as single-phase electrodes on both YSZ and CGO electrolytes and observed consistently lower resistances on CGO than on YSZ. The origin of the difference observed between the performances of the same electrode material on different electrolytes is not well understood. Lower interfacial transport resistance between electrode and electrolyte, wider triple phase boundary areas, or intermediate layers may all contribute. A more detailed understanding of the differences between different interfaces would seem to be critical to predicting performance and design of new systems.

One commonly used method for improving the performance of cathodes is to add a second phase of an ionic conductor to the electronically conducting electrode material. For example, YSZ is commonly added to LSM electrodes and results in a significantly lower electrode resistance. Composite cathodes have a high density of triple phase boundaries and at the appropriate composition continuous ionic and electronically conducting phases so that they have high ambipolar conductivity.[85] As an example, Murray and Barnett[86] compared 50 mol % LSM-YSZ composites with 50 mol % LSM-CGO composites (the optimum composition for 30% porosity). At 700 °C, the area resistance for YSZ was 4.92 ohm cm^2, whereas for CGO it was 1.06 ohm cm^2 consistent with the difference in the ionic conductivities. Clearly in situations where the electrode performance is limited by the ionic conductivity of the mixed conductor, the addition of a second phase of a better ionic conductor is advantageous even at the cost of the loss of some surface area for oxygen activation.

3.2.1. Specific Cathode Materials. Three oxide structure types have been studied as cathode materials: perovskite,[87] K_2NiF_4, and ordered double perovskites.

3.2.1.1. ABO_3 Perovskite Oxides. A significant number of oxide compositions with the perovskite structure have been investigated for use as cathode materials in intermediate temperature SOFCs with YSZ, CGO, and LSGM electrolytes. The perovskite lanthanum strontium manganite (LSM) is the most important electrode material in SOFCs and remains the practical choice for operation in the 700−900 °C range because of its high electrical conductivity, high electrochemical activity for the O_2 reduction reaction, high thermal stability, and compatibility with YSZ, GDC, and LSGM at operating conditions. Among cathode materials, LSM shows excellent microstructural stability and long-term performance stability. No doubt efforts will continue to improve its performance at lower operating temperatures. The current status of LSM can be found in a recent review by Jiang.[88]

For operation at lower temperatures with YSZ, A-site-doped lanthanum ferrite perovskites (LSF) with mixed electronic and ionic conductivities and adjustable thermal-expansion coefficients are promising cathode materials.[89−91] The studies on the solid-state reaction between Sr-doped lanthanum ferrite and YSZ with a barrier layer of CSO indicated no formation of insulating phases such as La- and Sr-zirconates up to 1400 °C.[92] Both A site doping of other alkaline earth metals and also B site doping, for example, aluminum- and nickel-doped LSF, have been studied.[93,94] Both of these materials were tested in single cell and half-cells and were not as active as the undoped LSF. Aluminum was thought to segregate to the surface where it reduced or blocked the number of active catalytic sites but did not change the intrinsic activity of the base LSF materials; nickel doping, on the other hand, decreased catalytic activity. Both studies tried to isolate intrinsic catalytic activity from electrode microstructure and illustrate the problem of understanding performance issues in the complex geometries needed for fuel cell operation.

Cobalt containing perovskites have high mixed electronic and ionic conductivities and exceptional electrochemical activity for oxygen reduction. Unfortunately they typically have high thermal-expansion coefficients, $> 20 \times 10^{-6}\ K^{-1}$, and react with YSZ at low temperatures (700 °C) to form insulating phases. Their use requires an intermediate

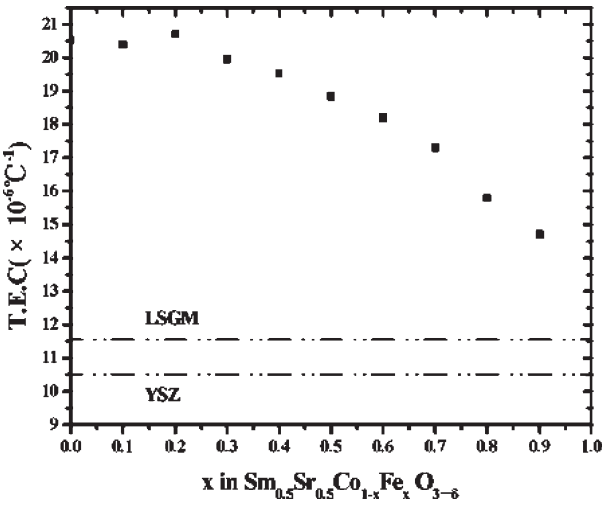

Figure 10. Variation in the thermal expansion coefficient of $Sm_{0.5}Sr_{0.5}Co_{1-x}Fe_xO_{3-x}$ with increasing iron content. Reprinted with permission from ref 100. Copyright 2006 Elsevier.

barrier layer, typically of doped ceria, and modification of the composition or the use of a composite to mitigate the effects of thermal expansion. The main application of cobaltites may be in SOFCs that use doped ceria as the electrolyte at temperatures in the 500−700 °C range where the kinetics of the oxygen reduction reaction limit the overall cell performance and cathodes with high catalytic activity are required. The cathode $La_{0.6}Sr_{0.4}Co_{0.2}Fe_{0.8}O_{3-x}$ is a good example of a composition developed for use with CGO operating at 550 °C.[95−97] The large iron content reduces the thermal expansion and the cobalt provides the catalytic "boost".

Two other perovskite compositions containing cobalt have shown exceptional performance in ceria or LSGM based SOFCs. $Sm_xSr_{1-x}CoO_3$ (SSC) has very good properties both as a single phase material and in SSC composite cathodes consisting of SSC−$La_{0.8}Sr_{0.2}Ga_{0.8}Mg_{0.2-x}Co_xO_3$ (LSGMC)[98] or SSC−$Gd_{0.1}Ce_{0.9}O_{1.95}$ (CGO).[99] Crystal structure, thermal expansion coefficient, electrical conductivity, and cathode polarization of $Sm_{0.5}Sr_{0.5}Co_{1-x}Fe_xO_{3-x}$ (SSCF) ($0 \le x \le 0.9$) series have also been studied. As in $La_{0.6}Sr_{0.4}Co_{0.2}Fe_{0.8}O_{3-x}$, the addition of iron reduces the thermal expansion coefficient (Figure 10).[100]

The second example, $Ba_{0.5}Sr_{0.5}Co_{0.8}Fe_{0.2}O_{3-x}$ (BSCF), was reported by Shao and Haile to give very low area specific resistances of 0.055−0.071 ohms cm^2 at 600 °C, and 0.51−0.60 ohms cm^2 at 500 °C in a $Sm_{0.2}Ce_{0.8}O_{1.9}$ (CSO)-electrolyte-based fuel cell.[101,102] The results have generated much interest and the system has been studied by several groups.[103−105] The current status of research on this material was recently reviewed by Zhou et al.[106] Interestingly, they have shown that the addition of silver improves the performance of BSCF electrodes; most of the previous work including the original report used silver in or as the current collectors. Silver is known to be extremely mobile in oxygen and has been observed to migrate to the electrolyte−electrode interface and this may have played some role in the excellent cathode performances reported.

3.2.1.2. K_2NiF_4 Structures. Oxides with the perovskite related K_2NiF_4 structure, for example, Ln_2NiO_{4+x}, (Ln = La, Pr, Nd) are of interest for SOFC cathodes because of the high diffusivity of the interstitial oxygen ions.[107] The structure of Ln_2NiO_{4+x} can be described as a succession of $LaNiO_3$ perovskite layers alternating with LaO rock salt layers. The oxygen excess in La_2NiO_{4+x} is associated with the incorporation of interstitial oxygen anions into the rock salt layers where they are tetrahedrally coordinated by La^{3+} cations. In La_2NiO_{4+x} at ambient temperature, x can be as high as 0.18 and in Pr_2NiO_{4+x}, the maximum value of x is 0.22. At higher temperature, the diffusivity increases though this is offset by the decrease in the concentration of oxygen interstitials. The advantages of lanthanum nickel oxide include in addition to high oxygen mobility a relatively low lattice expansion induced by variations in temperature and oxygen partial pressure.[108] The range of thermal expansion coefficients observed for the La_2NiO_4 compounds ($11-13 \times 10^{-6}\,K^{-1}$) matches reasonably well with the values for the electrolytes YSZ, CGO and LGSM.

As with the perovskite structure oxides, the Ln_2NiO_{4+x} compounds can incorporate chemical substitutions on both the La and Ni sites to give a wide range of different transport properties. Several systems have been investigated either by doping at the La position with alkaline-earths or by forming solid solutions of different rare earths.[109,110] Measurements of the surface exchange and self-diffusion coefficient were made for $La_{1-y}Sr_yNiO_{4+x}$, $y = 0.0, 0.1$, by isotope exchange and depth profiling in the temperature range 640−842 °C.[111] La_2NiO_{4+x} was found to have an oxygen diffusivity higher than that of $La_{0.6}Sr_{0.4}Co_{0.2}Fe_{0.8}O_{3-\delta}$ (LSCF) and 1 order of magnitude lower than the very good perovskite oxide mixed conductor $La_{0.3}Sr_{0.7}CoO_{3-\delta}$ (LSCO). The effects of strontium content on the electrical properties of $La_{2-x}Sr_xNiO_{4+x}$ have been reported.[112] The conductivity shows metallic behavior and increases with increasing strontium content reaching 273 S cm^{-1} at $x = 0.75$. For $(Pr,La)_2NiO_{4+x}$ solid solutions, impedance measurements in symmetric cells with YSZ as the electrolyte showed evidence for interfacial reaction between the electrode and electrolyte, and the resistances were an order of magnitude higher than for the same compounds on CGO. Substitution of Ni with other transition metals, for example, Cu and Co, has also been studied.[113−115] Although La_2NiO_{4+x} and related compounds have most of the intrinsic properties needed for a good cathode, the performance reported to date in SOFCs falls below expectations, therefore requiring further research.

The perovskite and K_2NiF_4 structure types are end members of a series of perovskite related intergrowth oxides of general formula $A_{n+1}B_nO_{3n+1}$ often referred to as Ruddlesden−Popper phases.[116] Iron and cobalt containing compositions exemplified by $(La,Sr)_{n+1}(Fe,Co)_nO_{3n+1}$ with $n = 2$ and $n = 3$ have been studied as cathodes and as oxygen permeation membranes.[117,118] The electrochemical performance of $Sr_{3-x}La_xFe_{2-y}Co_yO_{7-x}$, ($n = 2$), $LaSr_3Fe_{3-y}Co_yO_{10-x}$ ($n = 3$) have good

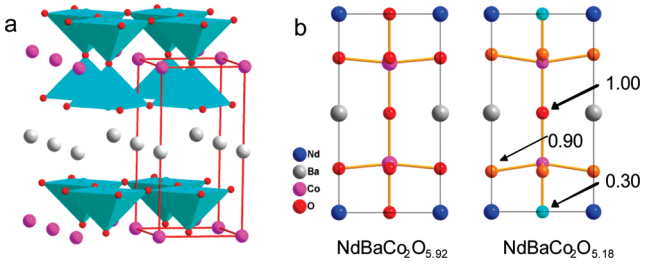

Figure 11. (a) Structure of $PrBaCo_2O_5$, Ba and Pr cations and oxygen anions, shown as purple, gray, and red spheres, respectively. The cobalt ion coordination is represented by the blue pyramids. (b) Comparison of the site occupancies of two $NdBaCo_2O_{5+x}$ compositions.

electrocatalytic activity for oxygen reduction in single cell measurements though the overall performance of $Sr_{3-x}La_xFe_{2-y}Co_yO_{7-x}$ is inferior to that of $LaSr_3Fe_{3-y}Co_yO_{10-x}$ ($n = 3$) most likely due to the decrease in electronic and ionic conductivities as the number of perovskite layers decreases. The lower performance is to some degree offset by the lower thermal expansion coefficient.

3.2.1.3. Ordered Double Perovskites. In the mixed conducting oxides represented by the general formula $AA'Co_2O_{5+x}$ (A = RE, Y and A′ = Ba, Sr),[119] the combination of rare earths and Ba or Sr on the A-site leads to A site ordering that is associated with rapid oxygen ion transport. These compounds are related to the "112" type structure first reported for $YBaFeCuO_5$[120] and consist of double layers of square pyramidally coordinated cobalt cations. The Ba^{2+} cations are located in the Co double layers, and these layers are separated by layers of lanthanide cations. The structures of representative examples, $PrBaCo_2O_{5+x}$ and $NdBaCo_2O_{5+x}$ ($x =$ 0.92, 0.18), of this class of compounds are shown in Figure 11.[121,122]

A considerable literature exists on the structural chemistry and low-temperature properties of the 112 phases including the cobalt compounds. In contrast, little was known concerning their high-temperature properties until Taskin et al.[123] measured high rates of oxygen uptake in $GdBaB_2O_{5+x}$ (B = Mn, Co), together with clear indications that the vacancy layers are important to this process. Independently, measurements on $PrBaCo_2O_{5+x}$ were made on both thin films[124] and bulk materials[125] and showed high oxygen diffusivity and rapid surface exchange kinetics. The measured rapid oxygen ion diffusion and surface exchange kinetics are reflected in the very low area specific resistance of electrodes containing $PrBaCo_2O_{5+x}$. At 600 °C, the measured value of the area specific resistance of a composite cathode was 0.15 ohms cm^2.[158]

In other studies[126−128] the electrode performance of $GdBaCo_2O_{5+x}$ has been investigated at temperatures below 700 °C by AC impedance spectroscopy. One potential problem with barium-containing systems is susceptibility to carbonate formation. Tarancon et al. studied the stability of $GdBaCo_2O_{5+x}$ and found very good stability in atmospheres of CO_2 (500 ppm to 100%) at temperatures up to 700 °C. Symmetric cells gave excellent performance with both CGO and LSGM electrolytes. Recently,[129] the performance of $REBaCo_2O_{5+x}$ (RE = La, Pr, Nd, Sm, and Eu) composite cathodes were determined in a CGO electrolyte-supported symmetrical cell arrangement. At a given temperature and oxygen partial pressure, the area specific resistance of the electrodes decreased as the ionic radius decreased from La to Eu. The electrode microstructures were not optimized but nevertheless the area specific resistances are low, for example, for the $EuBaCo_2O_{5+x}$ + CGO electrode ASR values of 0.095 ohm cm^2 at 700 °C and 0.49 ohm cm^2 at 600 °C were obtained. Manthiram and co-workers have also investigated the properties of $REBaCo_2O_{5+x}$ oxides with RE = Nd, Sm, Gd, and Y as cathodes in single-cell SOFCs fabricated with a LSGM electrolyte and $Ni-Ce_{0.9}Gd_{0.1}O_{1.95}$ cermet anodes. The power densities were observed to decrease with decreasing size of the rare earth ions ions, partly because of a decreasing electrical conductivity.[130] The same group has reported the effect of the substitution of Sr^{2+} ions for Ba^{2+} ions on the properties of $GdBa_{1-x}Sr_xCo_2O_{5+x}$. A structural change from orthorhombic ($x = 0$) to tetragonal ($0.2 < x < 0.6$) to orthorhombic ($x = 1$) was observed as the Sr content increased. The strontium ion substitution improves the chemical stability of cathodes in contact with both CGO and LSGM electrolytes. Compositions in the tetragonal composition range showed higher activity for oxygen reduction that the orthorhombic phases.[131]

The number of possible $AA'B_2O_{5+x}$ compositions that can be prepared is very large and only a small number have been examined so far. Recent examples include $YBaCo_2O_{5+x}$,[132] $LaBaCuFeO_{5+x}$, $LaBaCuCoO_{5+x}$[133] and $SmBa_{0.5}Sr_{0.5}Co_2O_{5+x}$.[134] Excellent area-specific resistance (ASR) values have been obtained with $SmBa_{0.5}Sr_{0.5}Co_2O_{5+x}$ electrodes in a symmetric cell using CGO. An ASR value of 0.092 ohm cm^2 at 700 °C was obtained. Even lower values (0.12 ohm cm^2 at 600 °C and 0.019 ohm cm^2 at 700 °C) were obtained for a 50:50 wt % composite with CGO on YSZ with a CGO interlayer. The coefficient of thermal expansion was reduced from $> 20 \times 10^{-6}\ K^{-1}$ to $13.6 \times 10^{-6}\ K^{-1}$ at 700 °C in the composite, a value more compatible with the other cell components. Substitution of Ni for cobalt in $NdBaCo_{2-x}Ni_xO_{5+x}$ has also been shown to reduce the thermal expansion coefficient to $16.7 \times 10^{-6}\ K^{-1}$ while maintaining the cathode performance in a single SOFC.[135]

The double perovskites are clearly an interesting class of cathode materials, but at this stage only limited data on a small number of compositions are available. More performance data under polarization conditions in complete cells are required, though some initial data for cathodes of $NdBaCo_2O_{5+x}$ and $PrBaCo_2O_{5+x}$ on a samarium-doped ceria electrolyte have been reported.[136,137]

3.3. Anodes. The literature on anode materials for solid oxide fuel cells is very extensive and can be only briefly summarized here. For more details, a number of excellent review articles are available.[138−144]

Usually, hydrogen is considered to be the primary fuel for fuel cells but in the case of SOFCs, because of their

high operating temperature, hydrocarbon fuels can be used directly. Because for the foreseeable future most hydrogen will come from reforming natural gas, liquid hydrocarbons or coal gasification, direct utilization has a significant efficiency advantage, though it does introduce further requirements on the anode material. Hydrocarbons such as methane can be fed directly to the cell (dry) or cofed with water (internal reforming). The latter requires higher operating temperatures because of the endothermic nature of steam reforming. In practice, some form of external reforming or partial oxidation is used to provide a mixture of hydrocarbons, hydrogen, and carbon monoxide to the cell. As discussed in section 2.2, the anode material has to satisfy a number of requirements including a stable microstructure, electronic and ionic conductivity, and catalytic activity. In addition, when operated on hydrocarbon fuels, they must be stable with respect to reactions with sulfur containing molecules and carbon dioxide. In general, the choice of anode (or cathode) depends on the specific electrolyte and finding an appropriate electrode may well determine the ultimate utility of a specific electrolyte. A detailed discussion of hydrocarbon oxidation mechanisms on SOFC anodes is beyond the present scope, but discussion of kinetics and mechanisms can be found in the references.[145,146]

The majority of anode research has concerned YSZ and Ni/YSZ cermets, which have been the anode of choice with this electrolyte for many years. The use of a cermet helps to match the thermal expansion coefficient and stabilize the microstructure. Because NiO does not form a solid solution with YSZ except at very high temperatures,[147] cermets can easily be made by cosintering NiO and YSZ followed by hydrogen reduction. Nickel is an excellent catalyst for both hydrogen oxidation and steam reforming. Unfortunately, it is sensitive to sulfur and catalyzes the formation of carbon fibers[148] by a mechanism that involves carbon deposition and subsequent dissolution in nickel particles.

Several approaches to limit carbon formation on anode materials have been taken. One approach is to lower the operating temperature. A cell in which an intermediate layer of yttria-doped ceria (CYO) was inserted between the YSZ electrolyte and the Ni/YSZ cermet was shown to directly electrochemically oxidize methane with power densities up to 0.37 Wcm^{-2} at 650 °C.[149] The performance was achieved by using both CYO and a low operating temperature to avoid carbon deposition. An alternate approach has been to replace the Ni component with Cu. Copper does not catalyze carbon formation and does not play a role in the electrocatalysis but it is effective as a current collector. To achieve reasonable power densities, it is necessary to add cerium oxide as an oxidation catalyst; Cu provides the electronic conductivity. Copper has a lower melting point than nickel, and consequently, Cu-containing anodes have to be used at lower temperature to avoid loss of surface area.[150,151]

One way of enhancing the activity and stability of Cu-based anodes involves alloying the Cu with a second metal such as Ni or Co that have higher catalytic activities. Kim et al.[152] examined the use of Cu−Ni alloys as anodes for the direct oxidation of methane in YSZ solid-oxide fuel cells at 800 °C and demonstrated that carbon formation is greatly suppressed on the alloys compared to pure Ni. In a similar way, anodes containing mixtures of Cu and Ni or Cu and Co showed improved performance in H_2 at 700 °C compared to Cu-based anodes and decreased carbon formation in n-butane compared to Ni- or Co-based anodes; the Cu−Co anode appeared to be more tolerant to carbon.[153] A number of other bi and trimetallic alloy systems in combination with ceria have also been investigated particularly in the context of materials with high activity in the intermediate temperature range. Examples include Ru/YSZ[154] Cu-CeO_2−SCSZ[155] and Ir/$Ce_{0.9}Gd_{0.1}O_{2-x}$.[156]

Recently, oxides with both electronic and ionic conductivity in the reducing atmosphere at the anode and which are catalytically more active than ceria for the oxidation of hydrocarbons have been evaluated as alternatives to metal-ceria based systems. A number of structure types have been considered including perovskite, pyrochlore, and spinel. As with cathode materials, the perovskite structure with its compositional flexibility and stability in the presence of a large number of oxygen vacancies provides an attractive option. Goodenough[84] has discussed the requirements for a suitable anode material, namely, the compound must have adequate electronic conductivity implying that the perovskite oxide remains mixed-valence in the reducing atmosphere at the anode, catalytic activity requires that the mixed valence redox couple can accept electrons from H_2 or the hydrocarbon fuel in order to induce dissociation on the oxide surface, and that the ionic conductivity is such that oxygen ions diffuse rapidly from the electrolyte to the surface of the anode. The difficulty to date has been finding a material that has the catalytic activity for hydrogen oxidation and methane reforming that is comparable to Ni, while having good mixed conductivity.

The most widely studied perovskites are the titanates and chromites because of their stability in reducing conditions. Strontium titanate ($SrTiO_3$) is a good electronic conductor at low oxygen partial pressures, so for application as an SOFC anode, it is doped to increase the ionic conductivity. The conductivity of $SrTiO_3$ increases when strontium is replaced with various lanthanides or with yttrium. Conductivities approaching 100 S cm^{-1} have been achieved.[157,158] Doping with niobium on the titanium site can also increase the conductivity.[159] The titanates also have been shown to have good dimensional and chemical stability upon redox cycling, but the electrocatalytic activity for H_2 oxidation is very poor.[160] However, it is possible to improve activity by introducing dopants such as Mn and Ga on the Ti site. In single-phase $La_4Sr_8Ti_{11}Mn_{0.5}Ga_{0.5}O_{37.5}$ under the reducing atmosphere at the anode, the Mn^{3+} is reduced to Mn^{2+} and some Ti^{4+} are reduced to Ti^{3+} to give electronic conductivity.[161] The oxygen vacancies introduced into the perovskite blocks give a high enough oxygen ion conductivity to replenish the O^{2-} ions on the oxide surface. This

composition shows impressive fuel-cell performance on wet hydrogen and is active for methane oxidation.[162] Similar results have been obtained with $La_{0.4}Sr_{0.6}Ti_{1-x}Mn_xO_{3-x}$.[163] Doped strontium titanate anodes have been shown to be tolerant to oxygen, carbon, and sulfur containing atmospheres.[164,165]

Doped $LaCrO_3$-based materials are used as interconnects in high-temperature SOFCs and are stable in reducing environments. Strontium-doped lanthanum chromite does not catalyze carbon deposition and thus can be used as an anode. The B-site of strontium-doped lanthanum chromite has been doped with various transition metals (Mn, Fe, Co, Ni, Cu) to introduce oxygen vacancies. Of these dopants, Ni gives the lowest polarization resistance, but has poor stability in low oxygen partial pressures. The perovskite system $(La_{1-x}Sr_x)Cr_{0.5}Mn_{0.5}O_{3-x}$ has shown good results for oxidation of wet H_2 and CH_4 at 900 °C, respectively.[166,167] The success of this oxide has led to its use with electrolytes in composite anodes for direct oxidation of methane[168,169] and to its use in an all perovskite SOFC.[170]

Recently, Goodenough and co-workers[171,172] reported that the double perovskite $Sr_2Mg_{1-x}Mn_xMoO_{6-x}$ could be used as an anode with natural gas as the fuel under operating temperatures 650 °C < T < 1000 °C with long-term stability and tolerance to sulfur. $Sr_2Mg_{1-x}Mn_xMoO_{6-x}$ is stable in reducing atmosphere retaining the double-perovskite structure when oxygen deficient. Measurement of the conductivity of polycrystalline $Sr_2Mg_{1-x}Mn_xMoO_{6-x}$ in an atmosphere of H_2 and CH_4 gave an electronic conductivity at 800 °C of 10 S cm^{-1}. Further modification of the double perovskite Sr_2MgMoO_{6-x} by La substitution has shown that $Sr_{2-x}La_xMgMoO_{6-x}$ with $0.6 \leq x \leq 0.8$ has even better performance as the anode of a solid oxide fuel cell.[173]

Althgouh impressive progress has been made in the development of alternative anode materials, significant problems remain, particularly with the low catalytic activity compared with nickel and the low electronic conductivity. Nevertheless, the desirable properties such as low carbon deposition and sulfur tolerance warrant their further study.

4. Summary and Future Directions

Several research areas have emerged over the past few years that are relevant to solid oxide fuel cells. These include continuing efforts to discover new compounds, nanostructured electrodes and electrolytes, in situ characterization techniques, and theoretical methods to predict ion migration paths and activation energies for diffusion. Atomistic simulations coupled with experiments are providing new insights into the defect chemistry and ion migration in complex oxides.[174−177]

Compounds where oxygen diffuses via an interstitial rather that a vacancy mechanism are one interesting class of new materials. The apatite structure electrolytes and the La_2NiO_{4+x} cathode materials are examples. Most recently the oxygen excess systems $CeMO_{4+x}$ (M = V, Nb, Ta) have also been shown to conduct oxygen via an interstitial mechanism. For example, $CeNbO_{4+x}$ with the fergusonite structure can accommodate oxygen excess up to a composition of $CeNbO_{4.25}$ in air. Measurements of the electrical properties show reasonably high total conductivities (0.03 S cm^2 at 850 °C) though the compound is a mixed conductor with an ionic transference number of 0.4.[178] The mixed conductivity is an indication of the complexity of the oxygen chemistry that can be present in interstitial systems. Some of the oxidation reactions that lead to interstitial oxygen atoms are shown schematically below to describe the resulting charge distributions

$$\text{metal centered} : V_i^{\times} + 1/2O_2 + 2M_M{}^{\times} = O_i^{''} + 2M_M^{\bullet}$$

$$\text{oxygen centered} : V_i^{\times} + 1/2O_2 + 2O_O{}^{\times} = O_i^{''} + 2O_O^{\bullet}$$

$$\text{oxidized oxygen} : O_i'' + 1/2O_2 = 2O_i' = O_i'' + 2h^{\bullet}$$

$$\text{peroxide formation} : O_i'' + 1/2O_2 = 2O_i' = O_{2i}''$$

An interesting example that illustrates the trade-off between oxidized oxygen and peroxide formation is La_2CuO_{4+x}. The relative contributions can be determined by measuring independently the total nonstoichiometry (x) by coulometric titration and the electron hole concentration from the thermopower. For compositions corresponding to $x > 0.03$, the addition of an interstitial oxygen atom contributes only 1.3 electron holes to the conduction band rather than the expected 2, indicative of the formation of some localized polyoxide species.[179] In a similar way, the highest oxygen interstitial concentration in La_2NiO_{4+x}, $x = 0.25$ was shown by neutron diffraction to contain $O_3{}^{5-}$ species.[180] An extreme example where only peroxide is formed is $Ba_5M_2O_{10}$ (M = Nb, Ru), which on oxidation forms $Ba_5M_2O_9O_2$, where all of the added oxygen is present as peroxide.[181]

A second area that is receiving increasing attention is the broad topic of nanionics. Nanostructured materials are characterized by short diffusion lengths, a high density of interfaces, and in some cases, where the interfaces are closely spaced, completely new properties are observed, as found for the transport properties of an artificial superlattice of CaF_2 and BaF_2.[182] A general discussion of the field of nanoionics can be found in the excellent review article by Maier,[183] and only a few examples are given here.

Porous electrodes are an example where reaction rates can be enhanced by increasing the number of interfaces and the effective electrode surface area. For example, cathodes containing nanoparticles have been prepared both by infiltration of porous electrodes and directly from presynthesized nanoparticles[184] with improved performance.[185] In a recent example, nanoporous $La_{0.5}Sr_{0.5}CoO_{3-x}$ cathodes with 8 nm particles were prepared on polycrystalline CGO by laser deposition and investigated by AC impedance spectroscopy. Even though the films were only 700 nm thick, they had very high surface

area ($80\,\mu m^{-1}$), showed stable behavior and had very low polarization resistances in the temperature range 500−700 °C.[83] Analysis of the results suggested that the enhanced performance was a consequence of the large surface area and not due to any fundamental modification of the materials properties. The use of nanostructured electrodes, provided that they can be stabilized against agglomeration, is a promising new direction.

Dense thin films prepared on electrolytes by physical vapor deposition may also be thought of as nanostructures. Thin films have mainly been used to provide electrode structures that are simpler than porous electrodes with the goal of using the well-defined geometry to determine more fundamental information about electrode reaction mechanisms. Thin films are also a necessary component of micro- solid oxide fuel cells and have been investigated for this application.[186,187] As an example, early studies of 250 nm dense thick films of $La_{0.5}Sr_{0.5}CoO_{3-x}$ on YSZ single crystal substrates in various oxygen pressures between 500−750 °C showed that the electrode reaction rate was limited entirely by the oxygen surface exchange reaction.[188,189] At this length scale, processes that involve surfaces and interfaces between components become dominant and one of the future challenges in the characterization of materials for microfuel cells and of electrocatalytic processes in general is to develop better understanding of the surface and interface chemistry under operating conditions. Several steps have recently been taken in this direction including in situ synchrotron X-ray studies,[190,191] variable-temperature static and magic angle spinning (MAS) ^{17}O NMR experiments,[192] pair distribution function analysis using neutron diffraction and X-ray diffraction data, and in situ infrared and Raman spectroscopy.[193]

Recent studies of $La_2Mo_2O_7$ are an excellent illustration of the level of detailed structural information that can now be obtained. Malavasi et al. used an atomic pair distribution analysis of the neutron scattering data including the diffuse scattering at 500 and 600 °C, above and below the phase transition, and demonstrated that the local structure of the high-temperature cubic phase is the same as that of the low-temperature monoclinic phase and that the phase transition corresponds to a transition from a static to a dynamic arrangement of the oxygen atoms.[194] The structure of the low-temperature ordered monoclinic phase was determined by single-crystal X-ray diffraction.[195] The structure is extraordinarily complex, containing 312 crystallographically distinct atoms in the unit cell. Evans et al. proposed that the high-temperature cubic structure could be considered as a time average of the room temperature monoclinic structure.

In conclusion, though much progress has been made in solid oxide fuel cell technology to the point where Ni/YSZ/YSZ/LSM cell stacks are approaching commercial viability, many opportunities remain for materials chemistry and the discovery of new compounds. Electrolytes with high stability, good mechanical properties, and better conductivity, efficient anodes for direct hydrocarbon conversion that are sulfur tolerant, and cathodes that catalyze the oxygen reduction reaction at lower temperatures are all important topics for future research. A solid oxide fuel cell is a complex device with solid−solid and gas−solid interfaces that must be stable over long periods at elevated temperature. The chemistry of the processes that occur at these interfaces such as ion transport and interdiffusion, changes in the surface structure and composition of the electrodes in response to changes in the environment including electric fields, and electrocatalytic pathways are all areas where deeper understanding will enhance our ability to design the next generation of SOFCs that will find practical application in distributed generation of electric power.

Acknowledgment. The author thanks the Robert A. Welch foundation and the department of Energy (DE-SC0001284) for financial support.

Glossary

ALS	Adler−Lane−Steele model
BiMeVOX	doped bismuth vanadate, $Bi_4V_{1.8}Cu_{0.2}O_{10.7}$
BSCF	barium strontium cobalt iron oxide
CGO	gadolinium-doped ceria
CSO	samarium-doped ceria
CYO	yttria-doped ceria
LaMOX	substituted $La_2Mo_2O_9$
LSCF	lanthanum strontium cobalt iron oxide
LSCO	lanthanum strontium cobalt oxide
LSF	doped lanthanum ferrite perovskites
LSGM	strontium, magnesium-doped lanthanum gallate
LSGMC	cobalt-doped LSGM
LSM	lanthanum strontium manganite, $La_{0.9}Sr_{0.1}MnO_3$
PBCO	praseodymium barium cobalt oxide
ScSZ	scandia-stabilized zirconia
SOFC	solid oxide fuel cell
SS	samarium strontium cobalt oxide
SSC	samarium strontium cobalt iron oxide
YS	yttria-stabilized zirconia

References

(1) Singhal, S. C. H.; Yokokawa, H.; *Solid Oxide Fuel Cells VII: Proceedings of the Seventh International Symposium*; Tsukuba, Japan, June 2001; The Electrochemical Society: Pennington, NJ, 2001.
(2) Minh, N. Q.; T. Takahashi, T. *Science and Technology of Ceramic Fuel Cells*; Elsevier, Amsterdam, 1995.
(3) Steele, B. C. H.; Heinzel, A. *Nature* **2001**, *414*, 345–352.
(4) Singh, P.; Pederson, L. R.; Simner, S. P.; Stevenson, J. W.; Viswanathan, V. V. *Proceedings of the 36th Intersociety Energy Conversion Engineering Conference*; Savannah, GA, July 29−Aug 2, 2001; ; American Society of Mechanical Engineers: New York, 2001, Vol. *2*, pp 953−958.
(5) Singhal, S. C. In *Solid Oxide Fuel Cells V: Proceeings of the 5th International Symposium*; Aachen, Germany, June 1997;Stimming, U., Singhal, S. C., Tagawa, H., Lehnert, W., Eds.; The Electrochemical Society: Pennington, NJ, 1997; pp 37−50.
(6) Kim, G.; Wang, S.; Jacobson, A. J.; Reimus, L.; Brodersen, P.; Mims, C. A. *J. Mater. Chem.* **2007**, *17*, 2500–2505.
(7) Ishihara, T.; Matsuda, H.; Takita, Y. *J. Am. Chem. Soc.* **1994**, *116*, 3801–3803.
(8) Steele, B. C. H. *Solid State Ionics* **2000**, *129*, 95–110.
(9) Steele, B. C. H. *Solid State Ionics* **1996**, *86−88*, 1223–1234.
(10) Huang, P.; Petric, A. *J. Electrochem. Soc.* **1996**, *143*, 1644–1648.
(11) Adler, S. B. *Chem. Rev.* **2004**, *104*, 4791–4843.
(12) Choi, Y.-M.; Mebane, D. S.; Wang, J.-H.; Liu, M. *Top. Catal.* **2007**, *46*, 386–401.

(13) Tao, S. W.; Irvine, J. T. S. *Chem. Rec.* **2004**, *4*, 83–95.
(14) Goodenough, J. B. *Annu. Rev. Mater. Res.* **2003**, *33*, 91–128.
(15) Moon, P. K.; Tuller, H. *Solid State Ionics* **1988**, *28*−*30*, 470–474.
(16) Abraham, F.; Boivin, J. C.; Mairesse, G.; Nowogrocki, G. *Solid State Ionics* **1990**, *40*−*41*, 934–937.
(17) Takahashi, T.; Iwahara, H.; Nagai, Y. *J. Appl. Electrochem.* **1972**, *2*, 97–104.
(18) Takahashi, T.; Iwahara, H.; Arao, T. *J. Appl. Electrochem.* **1975**, *5*, 187–195.
(19) Verkerk, M. J.; Keizer, K.; Burggraaf, A. J. *J. Appl. Electrochem.* **1980**, *10*, 81–90.
(20) Kruidhof, H.; Bouwmeester, H. J. M.; De Vries, K. J.; Gellings, P. J.; Burggraaf, A. J. *Solid State Ionics* **1992**, *50*, 181–186.
(21) Fung, K. Z.; Baek, H. D.; Virkar, A. V. *Solid State Ionics* **1992**, *52*, 199–211.
(22) Park, J.-Y.; Yoon, H.; Wachsman, E. D. *J. Am. Ceram. Soc.* **2005**, *88*, 2402–2408.
(23) Etsell, S T. H.; Flengas, S. N. *Chem. Rev.* **1970**, *70*, 339–336.
(24) Badwal, S. P. S. *Solid State Ionics* **1992**, *52*, 23–32.
(25) Solid State Energy Conversion Alliance http://www.netl.doe.gov/technologies/coalpower/fuelcells/seca/
(26) Badwal, S. P. S.; Foger, K. *Ceram. Int.* **1996**, *22*, 257–265.
(27) Badwal, S. P. S.; Ciacchi, F. T.; Milosevic, D. *Solid State Ionics* **2000**, *136*−*137*, 91–99.
(28) Arachi, Y.; Sakai, H.; Yamamoto, O.; Takeda, Y.; Imanishai, N. *Solid State Ionics* **1999**, *121*, 133–139.
(29) Politova, T. I.; Irvine, J. T. S. *Solid State Ionics* **2004**, *168*, 153–165.
(30) Inaba, H.; Tagawa, H. *Solid State Ionics* **1996**, *83*, 1–16.
(31) Mogensen, M.; Sammes, N. M.; Tompsett, G. A. *Solid State Ionics* **2000**, *129*, 63–94.
(32) Gong, W. Q.; Yadav, M.; Jacobson, A. J. unpublished results.
(33) Wang, S.; Kobayashi, T.; Dokiya, M.; Hashimoto, T. *J. Electrochem. Soc.* **2000**, *147*, 3606–3609.
(34) Wang, S.; Inaba, H.; Tagawa, H.; Hashimoto, T. *J. Electrochem. Soc.* **1997**, *144*, 4076–4080.
(35) Wang, S.; Kato, T.; Nagata, S.; Kaneko, T.; Iwashita, N.; Honda, T.; Dokiya, M. *Solid State Ionics* **2002**, *152*− *153*, 477–484.
(36) Van Herle, J.; Horita, T.; Kawada, T.; Sakai, N.; Yokokawa, H.; Dokiya, M. *J. Eur. Ceram. Soc.* **1996**, *16*, 961–973.
(37) Kudo, T.; Obayashi, H. *J. Electrochem. Soc.* **1975**, *122*, 142–147.
(38) Eguchi, K.; Setoguchi, T.; Inoue, T.; Arai, H. *Solid State Ionics* **1992**, *52*, 165–172.
(39) Wang, F.; Chen, S.; Wang, Q.; Yu, S.; Cheng, S. *Catal. Today* **2004**, *97*, 189–194.
(40) Wang, F. Y.; Chen, S. Y.; Cheng, S. *Electrochem. Commun.* **2004**, *6*, 743–746.
(41) Lubke, S.; Wiemhofer, H. D. *Solid State Ionics* **1999**, *117*, 229–243.
(42) Sha, X. Q.; Lu, Z.; Huang, X. Q.; Miao, J. P.; Jia, L. *J. Alloys Compd.* **2006**, *424*, 315–321.
(43) Guan, X.; Zhou, H.; Wang, Y.; Zhang, J. *J. Alloys Compd.* **2008**, *464*, 310–316.
(44) Mogensen, M.; Lybye, D.; Bonanos, N.; Hendriksen, P. V.; Poulsen, F. W. *Solid State Ionics* **2004**, *174*, 279–286.
(45) Jud, E.; Zhang, Z.; Sigle, W.; Gauckler, L. J. *J. Electroceram.* **2006**, *16*, 191–197.
(46) Zhang, T. S.; Ma, J.; Leng, Y. J.; Chan, S. H.; Hing, P.; Kilner, J. A. *Solid State Ionics* **2004**, *168*, 187–195.
(47) Hayashia, H.; Inaba, H.; Matsuyama, M.; Lan, N. G.; Dokiya, M.; Tagawa, H. *Solid State Ionics* **1999**, *122*, 1–15.
(48) Goodenough, J. B.; Ruiz-Diaz, J. E.; Zhen, Y. S. *Solid State Ionics* **1990**, *44*, 21–31.
(49) Prasanna, T. R. S.; Navrotsky, A. *J. Mater. Res.* **1993**, *8*, 1484–6.
(50) Cheng, J.; Navrotsky, A.; Zhou, X.-D.; Anderson, H. U. *Chem. Mater.* **2005**, *17*, 2197–2207.
(51) Goodenough, J. B.; Manthiram, A.; Paranthaman, P.; Zhen, Y. S. *Solid State Ionics* **1992**, *52*, 105–109.
(52) Manthiram, A.; Kuo, J. F.; Goodenough, J. B. *Solid State Ionics* **1993**, *62*, 225–234.
(53) Kakinuma, K.; Yamamura, H.; Haneda, H.; Atake, T. *Solid State Ionics* **2002**, *154*−*155*, 571–576.
(54) Kakinuma, K.; Arisaka, T.; Yamamura, H.; Atake, T. *Solid State Ionics* **2004**, *175*, 139–143.
(55) Ishihara, T.; Matsuda, H.; Takita, Y. *J. Am. Chem. Soc.* **1994**, *116*, 3801–3803.
(56) Ishihara, T.; Hiei, Y; Takita, Y. *Solid State Ionics* **1995**, *79*, 371–375.
(57) Feng, M.; Goodenough, J. B. *Eur. J. Solid State Inorg. Chem.* **1994**, *31*, 663–672.
(58) Huang, K.; Feng, M.; Goodenough, J. B. *J. Am. Ceram. Soc.* **1996**, *79*, 1100–104.
(59) Huang, K.; Tichy, R. S.; Goodenough, J. B. *J. Am. Ceram. Soc.* **1998**, *81*, 2565–2575.
(60) Huang, P.; Petric, A. *J. Electrochem. Soc.* **1996**, *143*, 1644–1648.
(61) Matraszeka, A.; Singheiser, L.; Kobertz, D.; Hilpert, K.; Miller, M.; Schulz, O.; Martin, M. *Solid State Ionics* **2004**, *166*, 343–350.
(62) Huang, K.; Tichy, R. S.; Goodenough, J. B. *J. Am. Ceram. Soc.* **1998**, *81*, 2576–2580.
(63) Yamaji, K.; Horita, T.; Ishikawa, M.; Sakai, N.; Yokokawa, H. *Solid State Ionics* **1999**, *121*, 217–224.
(64) Lacorre, P.; Goutenoire, F.; Bohnke, O.; Retoux, R.; Laligant, Y. *Nature* **2000**, *404*(6780), 856–858.
(65) Georges, S.; Goutenoire, F.; Altorfer, F.; Sheptyakov, D.; Fauth, F.; Suard, E.; Lacorre, P. *Solid State Ionics* **2003**, *161*, 231–241.
(66) Georges, S.; Goutenoire, F.; Laligant, Y.; Lacorre, P. *J. Mater. Chem.* **2003**, *13*, 2317–2321.
(67) Corbel, G.; Laligant, Y.; Goutenoire, F.; Suard, E.; Lacorre, P. *Chem. Mater.* **2005**, *17*, 4678–4684.
(68) Georges, S.; Goutenoire, F.; Bohnke, O.; Steil, M. C.; Skinner, S. J.; Wiemhoefer, H.-D.; Lacorre, P. *J. New Mater. Electrochem. Syst.* **2004**, *7*, 51–57.
(69) Marrero-Lopez, D.; Pena-Martinez, J.; Ruiz-Morales, J. C.; Perez-Coll, D.; Martin-Sedeno, M. C.; Nunez, P. *Solid State Ionics* **2007**, *178*, 1366–1378.
(70) Corbel, G.; Lacorre, P. *J. Solid State Chem.* **2006**, *179*, 1339–1344.
(71) Slater, P. R.; Sansom, J. E. H.; Tolchard, J. R. *Chem. Rec.* **2004**, *4*, 373–384.
(72) Kendrick, E.; Islam, M. S.; Slater, P. R. *J. Mater. Chem.* **2007**, *17*, 3104–3111.
(73) Iwata, T.; Bechade, E.; Fukuda, K.; Masson, O.; Julien, I.; Champion, E.; Thomas, P. *J. Am. Ceram. Soc.* **2008**, *91*, 3714–3720.
(74) Nakayama, S.; Aono, H.; Sadaokac, Y. *Chem. Lett.* **1995**, *6*, 431–432.
(75) Nakayama, S.; Kageyama, T.; Aono, H.; Sadaokac, Y. *J. Mater. Chem.* **1995**, *5*, 1801–1805.
(76) Nakayama, S.; Sakamoto, M.; Higuchi, M.; Kodaira, K.; Sato, M.; Kakita, S.; Suzuki, T.; Itoh, K. *J. Eur. Ceram. Soc.* **1999**, *19*, 507–510.
(77) Islam, M. S.; Tolchard, J. R.; Slater, P. R. *Chem. Commun.* **2003**, 1486–1487.
(78) Bechade, E.; Masson, O.; Iwata, T.; Julien, I.; Fukuda, K.; Thomas, P.; Champion, E. *Chem. Mater.* **2009**, *21*, 2508–2517.
(79) Tolchard, J. R.; Islam, M. S.; Slater, P. R. *J. Mater. Chem.* **2003**, *13*, 1956–1961.
(80) Jones, A.; Slater, P. R.; Islam, M. S. *Chem. Mater.* **2008**, *20*, 5055–5060.
(81) Shaula, A. L.; Kharton, V. V.; Marques, F. M. B. *Solid State Ionics* **2006**, *177*, 1725–1728.
(82) Adler, S. B.; Lane, J. A.; Steele, B. C. H. *J. Electrochem. Soc.* **1996**, *143*, 3554–3564.
(83) Wang, S.; Yoon, J.; Kim, G.; Huang, D.; Wang, H.; Jacobson, A. J. *Chem. Mater.* **2009**No. DOI:10.1021/cm9014139.
(84) Ralph, J. M.; Schoeler, A. C.; Krumpelt, M. *J. Mater. Sci.* **2001**, *36*, 1161–1172.
(85) Wu, Z.; Liu, M. *Solid State Ionics* **1997**, *93*, 65–84.
(86) Murray, E. P.; Barnett, S. A. *Solid State Ionics* **2001**, *143*, 265–273.
(87) Skinner, S. J. *Int. J. Inorg. Mater.* **2001**, *3*, 113–121.
(88) Jiang, S. P. *J. Mater. Sci.* **2008**, *43*, 6799–6833.
(89) Plonczak, P.; Gazda, M.; Kusz, B.; Jasinski, P. *J. Power Sources* **2008**, *181*, 1–7.
(90) Mai, A.; Haanappel, V. A. C.; Uhlenbruck, S.; Tietz, F.; Stöver, D. *Solid State Ionics* **2005**, *176*, 1341–1350.
(91) Simner, S. P.; Anderson, M. D.; Pederson, L. R.; Stevenson, J. W. *J. Electrochem. Soc.* **2005**, *152*, A1851–A1859.
(92) Simner, S. P.; Shelton, J. P.; Anderson, M. D.; Stevenson, J. W. *Solid State Ionics* **2003**, *161*, 11–18.
(93) Coffey, G. W.; Hardy, J.; Pedersen, L. R.; Rieke, P. C.; Thomsen, E. C.; Walpole, M. *Solid State Ionics* **2003**, *158*, 1–9.
(94) Coffey, G. W.; Hardy, J. S.; Pederson, L. R.; Rieke, P. C.; Thomsen, E. C. *Electrochem. Solid-State Lett.* **2003**, *6*, A121–A124.
(95) Bae, J.-M.; Steele, B. C. H. *Solid State Ionics* **1998**, *106*, 247–253.
(96) Oishi, N.; Atkinson, A.; Brandon, N. P.; Kilner, J. A.; Steele, B. C. H. *J. Am. Ceram. Soc.* **2005**, *88*, 1394–1396.
(97) Dusastre, V.; Kilner, J. A. *Solid State Ionics* **1999**, *126*, 163–174.
(98) Wang, S.; Chen, T.; Chen, S. *J. Electrochem. Soc.* **2004**, *151*, A1461–A1467.
(99) Xia, C.; Meilin Liu, M. *Solid State Ionics* **2001**, *144*, 249–255.
(100) Lv, H.; Wu, Y.-J.; Huang, B.; Zhao, B.; Hu, K. *Solid State Ionics* **2006**, *177*, 901–906.
(101) Shao, Z. P.; Haile, S. M. *Nature* **2004**, *43*, 170–173.
(102) Shao, Z. P.; Haile, S. M.; Ahn, J.; Ronney, P. D.; Zhan, Z. L.; Barnett, S. A. *Nature* **2005**, *435*, 795–798.
(103) Chen, Z. H.; Ran, R.; Zhou, W.; Shao, Z. P.; Liu, S. M. *Electrochim. Acta* **2007**, *52*, 7343–7351.
(104) Wang, K.; Wang, K.; Wang, K.; Wang, K.; Wang, K. *J. Power Sources* **2008**, *179*, 60–68.
(105) Wang, K.; Ran, R.; Zhou, W.; Gu, H. X.; Shao, Z. P.; Ahn, J. *J. Power Sources* **2008**, *179*, 60–68.
(106) Zhou, W.; Ran, R.; Shao, Z. *J. Power Sources* **2009**, *192*, 231–246.
(107) Kharton, V. V.; Yaremchenko, A. A.; Shaula, A. L.; Patrakeev, M. V.; Naumovich, E. N.; Logvinovich, D. I.; Frade, J. R.; Marques, F. M. B. *J. Solid State Chem.* **2004**, *177*, 26–37.
(108) Yaremchenko, A. A.; Kharton, V. V.; Patrakeev, M. V.; Frade, J. R. *J. Mater. Chem.* **2003**, *13*, 1136–1144.
(109) Wan, J.; Goodenough, J. B.; Zhu, J. H. *Solid State Ionics* **2007**, *178*, 281–286.

(110) Kim, G.; Jacobson, A. J. *Mater. Res. Soc. Symp. Proc.* **2007**, *972*, 175–180.
(111) Skinner, S. J.; Kilner, J. A. *Solid State Ionics* **2000**, *135*, 709–712.
(112) Aguadero, A.; Escudero, M. J.; Perez, M.; Alonso, J. A.; Pomjakushin, V.; Daza, L. *Dalton Trans.* **2006**, 4377–4383.
(113) Mauvy, F.; Bassat, J. M.; Boehm, E.; Dordor, P.; Loup, J. P. *Solid State Ionics* **2003**, *158*, 395–407.
(114) Aguadero, A.; Alonso, J. A.; Escudero, M. J.; Daza, L. *Solid State Ionics* **2008**, *179*, 393–400.
(115) Munnings, C. N.; Skinner, S. J.; Amow, G.; Whitfield, P. S.; Davidson, I. J. *Solid State Ionics* **2005**, *176*, 1895–1901.
(116) Popper, P.; Ruddlesden, S. N. *Trans. Brit. Ceram. Soc.* **1963**, *62*, 443–449.
(117) Lee, K. T.; Bierschenk, D. M.; Manthiram, A. *J. Electrochem. Soc.* **2006**, *153*, A1255–A1260.
(118) Lee, K. T.; Manthiram, A. *Chem. Mater.* **2006**, *18*, 1621–1626.
(119) Maignan, A.; Martin, C.; Pelloquin, D.; Nguyen, N.; Raveau, B. *J. Solid State Chem.* **1999**, *142*, 247–260.
(120) Caignaert, V.; Mirebeau, I.; Bouree, F.; Nguyen, N.; Ducouret, A.; Greneche, J.-M.; Raveau, B. *J. Solid State Chem.* **1995**, *114*, 24–35.
(121) Pralong, V.; Caignaert, V.; Hebert, S.; Maignan, A.; Raveau, B. *Solid State Ionics* **2006**, *177*, 1879–1881.
(122) Frontera, C.; Caneiro, A.; Carrillo, A. E.; Oro-Sole, J.; Garcia-Munoz, J. L. *Chem. Mater.* **2005**, *17*, 5439–5445.
(123) Taskin, A. A.; Lavrov, A. N.; Ando, Yoichi. *Appl. Phys. Lett.* **2005**, *86*, 091910/1–091910/3.
(124) Yuan, Z.; Liu, J.; Chen, C. L.; Wang, C. H.; Luo, X. G.; Chen, X. H.; Kim, G. T.; Huang, D. X.; Wang, S. S.; Jacobson, A. J.; Donner, W. *Appl. Phys. Lett.* **2007**, *90*, 212111/1–212111/3.
(125) Kim, G.; Wang, S.; Jacobson, A. J. Novel cathode and electrolyte materials for solid oxide fuel cells and ion transport membranes. US PSN: 60/706 836, **2005**.
(126) Chang, A.; Skinner, S. J.; Kilner, J. A. *Solid State Ionics* **2006**, *177*, 2009–2011.
(127) Tarancon, A.; Pena-Martinez, J.; Marrero-Lopez, D.; Morata, A.; Ruiz-Morales, J. C.; Nunez, P. *Solid State Ionics* **2008**, *179*, 2372–2378.
(128) Tarancon, A.; Skinner, S. J.; Chater, R. J.; Hernandez-Ramirez, F.; Kilner, J. A. *J. Mater. Chem.* **2007**, *17*, 3175–3181.
(129) Gong, W.; Yadav, M.; Jacobson A. J. Mater. Res Soc. Symp. Proc. **2009**, *1126*.
(130) Kim, J.-H.; Manthiram, A. *J. Electrochem. Soc.* **2008**, *155*, B385–B390.
(131) Kim, J.-H.; Prado, F.; Manthiram, A. *J. Electrochem. Soc.* **2008**, *155*, B1023–B1028.
(132) Liu, Y. *J. Alloys Compd.* **2009**, *477*, 860–862.
(133) Zhou, Q.; He, T.; He, Q.; Ji, Y. *Electrochem. Commun.* **2009**, *11*, 80–83.
(134) Kim, J. H.; Cassidy, M.; Irvine, J. T. S.; Bae, J. *J. Electrochem. Soc.* **2009**, *156*, B682–B689.
(135) Kim, J.-H.; Manthiram, A. *Electrochim. Acta* **2009**, *54*, 7551–7557.
(136) Gu, H.; Chen, H.; Gao, L.; Zheng, Y.; Zhu, X.; Guo, L. *Int. J. Hydrogen Energy* **2009**, *34*, 2416–2420.
(137) Chen, D.; Ran, R.; Zhang, K.; Wang, J.; Shao, Z. *J. Power Sources* **2009**, *188*, 96–105.
(138) Goodenough, J. B.; Huang, Y.-H. *J. Power Sources* **2007**, *173*, 1–10.
(139) Sun, C.; Stimming, U. *J. Power Sources* **2007**, *171*, 247–260.
(140) Gross, M. D.; Vohs, J. M.; Gorte, R. J. *J. Mater. Chem.* **2007**, *17*, 3071–3077.
(141) Sarantaridis, D.; Atkinson, A. *Fuel Cells* **2007**, *7*, 246–258.
(142) Fergus, J. W. *Solid State Ionics* **2006**, *177*, 1529–1541.
(143) Tao, S. W.; Irvine, J. T. S. *Metal Oxides: Chemistry and Applications*; Chemical Industries; CRC Press: Boca Raton, FL, 2006; Vol. *108*, pp 739−765.
(144) Atkinson, A.; Barnett, S.; Gorte, R. J.; Irvine, J. T. S.; McEvoy, A. J.; Mogensen, M.; Singhal, S. C.; Vohs, J. *Nat. Mater.* **2004**, *3*, 17–27.
(145) Mogensen, M. *Proceedings of the 26th Risø International Symposium on Materials Science*; Roskilde, Denmark, Sept 4−8, 2005; Linderoth, S., Ed.; Risø National Laboratory for Sustainable Science, Technical University of Denmark: Roskilde, Denmark, 2005; pp 51−66.
(146) McIntosh, S.; Gorte, R. J. *Chem. Rev.* **2004**, *104*, 4845–4865.
(147) Gerk, C.; Willert-Porada, M. *Innovative Materials in Advanced Energy Technologies*; Advances in Science and Technology; Techna: Faenza, Italy, 1999; Vol. *24*, pp 71−78.
(148) Keep, C. W.; Baker, R. T. K.; France, J. A. *J. Catal.* **1977**, *47*, 232–238.
(149) Murray, E. P.; Tsai, T.; Barnett, S. A. *Nature* **1999**, *400*(6745), 649–651.
(150) Park, S.; Vohs, J. M.; Gorte, R. J. *Nature* **2000**, *404*(6775), 265–267.
(151) Gorte, R. J.; Park, S.; Vohs, J. M.; Wang, C. *Adv. Mater.* **2000**, *12*, 1465–1469.
(152) Kim, H.; Lu, C.; Worrell, W. L.; Vohs, J. M.; Gorte, R. J. *J. Electrochem. Soc.* **2002**, *149*, A247–A250.
(153) Lee, S.-I.; Ahn, K.; Vohs, J. M.; Gorte, R. J. *Electrochem. Solid-State Lett.* **2005**, *8*, A48–A51.
(154) Zhan, Z.; Barnett, S. A. *Science* **2005**, *308*(5723), 844–847.
(155) Ye, X.-F.; Huang, B.; Wang, S. R.; Wang, Z. R.; Xiong, L.; Wen, T. L. *J. Power Sources* **2007**, *164*, 203–209.
(156) Wisniewski, M.; Boréave, A.; Gélin, P. *Catal. Commun.* **2005**, *6*, 596–600.
(157) Hui, S.; Petric, A. *J. Eur. Ceram. Soc.* **2002**, *22*, 1673–1681.
(158) Hui, S.; Petric, A. *J. Electrochem. Soc.* **2002**, *149*, J1–J10.
(159) Blennow, P.; Hansen, K. K.; Wallenberg, L. R.; Mogensen, M. *Solid State Ionics* **2009**, *180*, 63–70.
(160) Marina, O. A.; Canfield, N. L.; Stevenson, J. W. *Solid State Ionics* **2002**, *149*, 21–28.
(161) Escudero, J.; Irvine, J. T. S.; Daza, L. *J. Power Sources* **2009**, *192*, 43–50.
(162) Ruiz-Morales, J. C.; Canales-Vázquez, J.; Savaniu, C.; Marrero-López, D.; Zhou, W.; Irvine, J. T. S. *Nature* **2006**, *439*, 568–571.
(163) Fu, Q. X.; Tietz, F.; D. Stöver, D. *J. Electrochem. Soc.* **2006**, *153*, D74–D83.
(164) Mukundan, R.; Brosha, E. L.; Garzon, F. H. *Electrochem. Solid-State Lett.* **2004**, *7*, A5–A7.
(165) Cheng, Z.; Zha, S.; Liu, M. *J. Electrochem. Soc.* **2006**, *153*, A1302–A1309.
(166) Tao, S. W.; Irvine, J. T. S. *Nat. Mater.* **2003**, *2*, 320–323.
(167) Tao, S. W.; Irvine, J. T. S. *J. Electrochem. Soc.* **2004**, *151*, A252–A259.
(168) Kim, G.; Corre, G.; Irvine, J. T. S.; Vohs, J. M.; Gorte, R. J. *Electrochem. Solid-State Lett.* **2008**, *11*, B16–B19.
(169) Jiang, S. P.; Chen, X. J.; Chan, S. H.; Kwok, J. T.; Khor, K. A. *Solid State Ionics* **2006**, *177*, 149–157.
(170) Tao, S. W.; Irvine, J. T. S.; Kilner, J. A. *Adv. Mater.* **2005**, *17*, 1734–1737.
(171) Huang, Y.-H.; Dass, R. I.; Xing, Z.-L.; Goodenough, J. B. *Science* **2006**, *312*, 254–257.
(172) Huang, Y.-H.; Dass, R. I.; Denyszyn, J. C.; Goodenough, J. B. *J. Electrochem. Soc.* **2006**, *153*, A1266–A1272.
(173) Ji, Y.; Huang, Y.-H.; Rong Ying, J.-R.; Goodenough, J. B. *Electrochem. Commun.* **2007**, *9*, 1881–1885.
(174) Lee, Y.-L.; Morgan, D. *Mater. Res. Soc. Symp. Proc.* **2007**, *972*, 71–76.
(175) Rupasov, D.; Chroneos, A.; Parfitt, D.; Kilner, J. A.; Grimes, R. W.; Istomin, S. Ya.; Antipov, E. V. *Phys. Rev. B* **2009**, *79*, 172102/1–172102/4.
(176) Cleave, A. R.; Kilner, J. A.; Skinner, S. J.; Murphy, S. T.; Grimes, R. W. *Solid State Ionics* **2008**, *179*, 823–826.
(177) Jones, A.; Islam, M. S. *J. Phys. Chem. C* **2008**, *112*, 4455–4462.
(178) Packer, R. J.; Skinner, S. J.; Yaremchenko, A. A.; Tsipis, E. V.; Kharton, V. V.; Patrakeev, M. V.; Bakhteeva, Yu. A. *J. Mater. Chem.* **2006**, *16*, 3503–3511.
(179) Li, Z. G.; Feng, H. H.; Yang, Z. Y.; Hamed, A.; Ting, S. T.; Hor, P. H.; Bhavaraju, S.; DiCarlo, J. F.; Jacobson, A. J. *Phys. Rev. Lett.* **1996**, *77*, 5413–5416.
(180) Demourgues, A.; Weill, F.; Darriet, B.; Wattiaux, A.; Grenier, J. C.; Gravereau, P.; Pouchard, M. *J. Solid State Chem.* **1993**, *106*, 330–338.
(181) Grasset, F.; Dussarrat, C.; Darriet, J. *J. Mater. Chem.* **1997**, *7*, 1911–1915.
(182) Sata, N.; Eberman, K.; Eberl, K.; Maler, J. *Nature* **2000**, *408*(6815), 946–949.
(183) Maier, J. *Nat. Mater.* **2005**, *4*, 805–815.
(184) Sholklapper, T. Z.; Jacobson, C. P.; Visco, S. J.; De Jonghe, L. C. *Fuel Cells* **2008**, *8*, 303–312.
(185) Peters, C.; Weber, A.; Ivers-Tiffee, E. *J. Electrochem. Soc.* **2008**, *155*, B730–B737.
(186) Fleig, J.; Tuller, H. L.; Maier, J. *Solid State Ionics* **2004**, *174*, 261–270.
(187) Beckel, D.; Muecke, U. P.; Schoeberle, B.; Mueller, P.; Gauckler, L. J. *Thin Solid Films* **2009**, *517*, 1582–1586.
(188) Yang, Y. L.; Chen, C. L.; Chen, S. Y.; Chu, C. W.; Jacobson, A. J. *J. Electrochem. Soc.* **2000**, *147*, 4001–4007.
(189) Mims, C. A.; Joos, N. I.; van der Heide, P. A. W.; Jacobson, A. J.; Chen, C. L.; Chu, C. W.; Kim, B. I.; Perry, S. S. *Electrochem. Solid-State Lett.* **2000**, *3*, 59–61.
(190) Kim, G.; Wang, S.; Jacobson, A. J.; Yuan, Z.; Donner, W.; Chen, C. L.; Reimus, L.; Brodersen, P.; Mims, C. A. *Appl. Phys. Lett.* **2006**, *88*, 024103/1–024103/3.
(191) Fister, T. T.; Fong, D. D.; Eastman, J. A.; Baldo, P. M.; Highland, M. J.; Fuoss, P. H.; Balasubramaniam, K. R.; Meador, J. C.; Salvador, P. A. *Appl. Phys. Lett.* **2008**, *93*, 151904/1–151904/3.
(192) Holmes, L.; Peng, L.; Heinmaa, I.; O'Dell, L. A.; Smith, M. E.; Vannier, R.-N.; Grey, C. P. *Chem. Mater.* **2008**, *20*, 3638–3648.
(193) Lu, X. Y.; Faguy, P. W.; Liu, M. *J. Electrochem. Soc.* **2002**, *149*, A1293–A1298.
(194) Malavasi, L.; Kim, H. J.; Billinge, S. J. L.; Proffen, T.; Tealdi, C.; Flor, G. *J. Am. Chem. Soc.* **2007**, *129*, 6903–6907.
(195) Evans, I. V.; Howard, J. A. K.; Evans, J. S. O. *Chem. Mater.* **2005**, *17*, 4074–4077.